Energy Conversion and Management 153 (2017) 538–556

Contents lists available at ScienceDirect

Energy Conversion and Management

journal homepage: www.elsevier.com/locate/enconman

Thermodynamic evaluation and multi-objective optimization of molten carbonate fuel cell-supercritical CO_2 Brayton cycle hybrid system

Mohammad Ali Jokar[a], Mohammad H. Ahmadi[b,*], Mohsen Sharifpur[c], Josua P. Meyer[c], Fathollah Pourfayaz[a,*], Tingzhen Ming[d]

[a] Department of Renewable Energy and Environmental Engineering, University of Tehran, Tehran, Iran
[b] Faculty of Mechanical Engineering, Shahrood University of Technology, Shahrood, Iran
[c] Department of Mechanical and Aeronautical Engineering, University of Pretoria, Pretoria, South Africa
[d] School of Civil Engineering and Architecture, Wuhan University of Technology, Wuhan, PR China

ARTICLE INFO

Keywords:
Molten carbonate fuel cell (MCFC)
Supercritical carbon dioxide Brayton cycle
Exergy-based ecological function
Sensitivity analysis
Multi-disciplinary approach

ABSTRACT

Fuel cell-heat engine hybrid system is a relatively new discipline which proposes to utilize the excess high-temperature heat of the fuel cell as the heat source for the heat engine. This paper is concerned with a thermodynamic analysis of a molten carbonate fuel cell-SCO_2 Brayton hybrid system to optimize its performance based on a list of criteria. Four objective functions are considered, including energy efficiency, power density, exergy destruction rate density and ecological function density, to study the influence of four main parameters, including compressor inlet temperature and turbine inlet temperature of the Brayton cycle, and interconnect plate area and current density of the fuel cell, on the performance of the hybrid cycle. The strong conflict between the objective functions necessitates a multi-objective optimization procedure and, therefore, three scenarios are proposed, each takes into account a combination of three of these objective functions. The multi-objective evolutionary method integrated with non-dominated sorting genetic algorithm is used to obtain Pareto optimal frontiers. Finally, three efficient decision-making tools including TOPSIS, LINMAP and Fuzzy are employed by means of which the best answers in each case scenario are selected.

Examining the Fuzzy method results for example, in the first scenario, which doesn't consider power density, ecological function density and exergy destruction rate density meet their optimum values, 1.314 and 0.3864 kW/m^2, respectively. However, energy efficiency falls by 10% compared to its maximum, which occurs in the third scenario (0.6676), where ecological function density isn't included, and power density drops by 25% compared to its own in the second scenario (2.2783 kW/m^2), where energy efficiency is not. This indicates the strong confliction between the objective functions and also the necessity of this kind of analysis. However, the first scenario would roughly provide the best condition for the system if one wanted all the objective functions to be optimum all together.

1. Introduction

Fuel cells (FCs) have been the main subject of many studies during the last decades stemming from an increasing worldwide concern on environmental pollution, global warming, and energy sources. In addition to their inherently clean, efficient, and reliable services, FCs are capable of being coupled with different thermal cycles providing more efficient options. Various types such as solid oxide fuel cell (SOFC), molten carbonate fuel cell (MCFC), proton exchange membrane fuel cell (PEMFC), phosphoric acid fuel cell (PAFC) and direct carbon fuel cell (DCFC) are examined and represented in the literature [1–5]. However, these systems can still be examined from different points of view. Thermodynamic evaluation and numerical investigation on thermal performance can be a perfect tool for identifying the ways of improving the efficiency of thermal systems [6–10]. Zhao et al. [1] developed a thermodynamic model to study an irreversible SOFC, using the theory of electrochemistry and non-equilibrium thermodynamics. Zhang et al. [3] analyzed MCFC form thermodynamic-electrochemical point of view and derived useful expressions for computing main parameters of the fuel cell, including cell voltage, power output, efficiency, and entropy production rate. They also used a multi-optimization method enabling to consider the energy efficiency and power output concurrently.

To further grow FCs' future market, different solutions have been

* Corresponding authors.
E-mail addresses: mhosein.ahmadi@shahroout.ac.ir, mohammadhosein.ahmadi@gmail.com (M.H. Ahmadi), pourfayaz@ut.ac.ir (F. Pourfayaz).

https://doi.org/10.1016/j.enconman.2017.10.027
Received 29 July 2017; Received in revised form 8 October 2017; Accepted 9 October 2017
Available online 18 October 2017
0196-8904/

Nomenclature

A	area (m^2)
C	heat capacity (W/K)
e	ecological function density (W/m^2)
E	ecological function (W)
En_{act}	activation energy (J/mol^2)
exd	exergy destruction rate density (W/m^2)
Exd	exergy destruction rate (W)
F	Faraday constant (C/mol)
g	molar Gibbs free energy (J/mol)
$\Delta\dot{G}$	change of Gibbs free energy rate (W)
h	molar enthalpy (J/mol)
Δh	molar enthalpy change (J/mol)
$-\Delta\dot{H}$	change of enthalpy rate (W)
j	current density (A/m^2)
k	ratio of specific heats
K	heat conductance ($W/m^2{\cdot}K$)
n_e	number of electrons
p	pressure (atm)
p	power density (W/m^2)
P	power (W)
$\dot{Q}$	heat rate (W)
R	universal gas constant (J/mol·K)
T	temperature (K)
U	potential (V)
x	isentropic temperature

Subscripts

an	anode
B	Brayton
C	fuel cell
cat	cathode
CO_2	carbon dioxide
cp	compression
ex	expansion
h	hot side
H	hybrid
H_2	hydrogen
H_2O	water
i	ideal standard
l	cold side
max	maximum
o	environmental condition
O_2	oxygen
ohm	ohm overpotential
r	regenerator
rc	recuperator
rev	reversible
s	isentropic condition
SCO_2	supercritical carbon dioxide cycle
t	theoretical maximum potential

Greek letters

η	energy efficiency
ε	effectiveness

Abbreviations

C	compressor
DCFC	direct carbon fuel cell
FC	fuel cell
FTT	finite time thermodynamic
GA	genetic algorithm
GT	gas turbine
HE	heat exchanger
MCFC	molten carbonate fuel cell
MOEA	multi-objective evolutionary algorithm
MOO	multi-objective optimization
NSGA	non-dominated sorting genetic algorithm
PAFC	phosphoric acid fuel cell
PEMFC	proton exchange membrane fuel cell
Rec	recuperator
Reg	regenerator
SCO_2	super critical carbon dioxide
SOFC	solid oxide fuel cell
T	turbine

investigated. As one with the most promising results, hybridization of fuel cells has been advanced by which excessive heat rejected of high temperature is recovered in order to improve the energy efficiency. It has been shown that different configurations of fuel cell-heat engine hybrid systems are practicable [11–30]. SOFC and MCFC work at high temperature and, therefore, are more appropriate for these applications. Zhang et al. [16] developed a model taking into account multi-irreversibilities of a hybrid MCFC-heat engine system and their influence on the performance of the system. In a similar manner, the optimal performance of a hybrid system consisting of MCFC and gas turbine was discussed by determining the power output and efficiency expressions [18]. Chen et al. [21] studied an MCFC-Stirling engine hybrid system and showed the efficiency improvement of the hybrid system because of the coupling. They also investigated the performance dependency of the hybrid system to main operating conditions, including operating temperature, partial pressure of gases in anode and cathode and operating pressure. The upper and lower bounds of the objective functions were determined as well. In another study, Zhang et al. [26] developed a model describing the general characteristic of an MCFC-gas turbine hybrid system with direct internal reforming. In the proposed system, the auxiliary burner served as a high-temperature heat reservoirs of the Brayton cycle.

Among the different configurations, conventional Brayton cycle has been proved to be one of the most practical bottom-cycle. Since these systems are more compact compared with steam systems lower capital cost is required. In SCO_2 Brayton cycles, CO_2 above its critical point is applied as the working fluid. Due to thermodynamic conditions of the working fluid, there is significant decrease in compressor work, which results in higher efficiency of the cycle. Some of the studies conducted on hybrid MCFC-SCO_2 Brayton heat engines are represented in Refs. [31–35]. In Refs. [31,32], SCO_2 and air Brayton-MCFC hybrid systems are compared and it was observed that SCO_2 Brayton cycle-MCFC hybrid system is more favorable both in efficiency and output power. Mahmoudi and Ghavimi [34], conducted a study on MCFC-SCO_2 Brayton-organic Rankine cycle hybrid system and applied thermo-economic and multi objective optimization methods to analyze the system performance. Obtained results showed that exergy efficiency could be achieved up to 65.3% and product unit cost decreased to 0.039 cent (US/kWh). In another study, MCFC-SCO_2 Brayton hybrid system was compared with MCFC-organic Rankine cycle hybrid system [33]. Results indicated that by applying SCO_2 Brayton hybrid system as a bottoming cycle, compared with organic Rankine cycle, approximately 5% increase in energy efficiency was reachable. In Ref. [35], exergy analysis was conducted on MCFC-SCO_2 Brayton cycle. Result showed that overall energy and exergy efficiency of the system were 78% and 50%, respectively. In addition, it was found that exergy efficiency of reformer

was minimum while exergy efficiency of E-101 heat exchanger was maximum.

One of the best tools in order to assess thermodynamic cycles and complex systems is Finite-Time-Thermodynamics (FTT). In this approach, internal and external irreversibilities are considered; therefore analysis and optimization are more realistic. Various thermodynamic cycles, Carnot [36,37], Brayton [38–43], Stirling engine [44], SOFC [45], etc. [46–55], are explored by this rigorous methodology. Angulo-Brown proposed an ecological function [56] and it was modified later by Yan [57]. The function application in Brayton cycles can be further seen in Refs. [58–68]. Exergetic sustainability index is another criterion which is used in order to assess sustainability of thermal cycles [69–80].

Multi-objective optimization (MOO) is an increasingly popular and reliable solver applied in various engineering studies [81–85]. The idea is to consider various targets simultaneously and to apply effective optimization techniques in order to attain the overall optimal performance of a complex system. Blecic et al. [82] combined Bayesian analysis and multi-objective evolutionary algorithm (MOEA) and presented a model called Bay MODE. By applying this tool and evolutionary methods, a model for future prediction is proposed by Özyer et al. [83]. MOEA is generally applied to define a collection of solutions called Pareto frontier, the solutions which best satisfy the objective functions all together [86–88]. MOEA is also utilized in a variety of energy-related studies [89–122]. Autissier et al. [91] conducted a multi-objective thermo-economic optimization on a SOFC-GT hybrid system. The goal of the optimization was minimizing capital cost of system and maximizing its electricity generation efficiency. Ahmadi et al. [92,93] applied artificial intelligence and proposed novel model to obtain output power of solar-based Stirling heat engine. In other studies [95,105] NSGA-II was used to conduct optimization in a solar-driven heat engine and a heat pump economically and thermodynamically. Toghyani [98] applied non-ideal adiabatic approaches to investigate the performance of Stirling engine. Other models were presented to assess the cooling load of Stirling cryogenic refrigerator cycle [99]. Sayyaadi et al. [101] optimized design components of a Solar-Driven Heat Engine by NSGA-II. Ahmadi et al. [104] investigated an irreversible three-heat-source absorption heat pump thermodynamically and used MOEA for its optimization. MOEA and thermos-economic analysis were utilized for optimization of irreversible regenerative closed Brayton cycle and an endoreversible Braysson cycle [108,111].

In this study, an MCFC-SCO_2 Brayton heat engine is analyzed and, underlying importance of environmental criteria, ecological function is applied to obtain the optimum performance. Ecological function includes power output, energy efficiency and exergy destructions as thermodynamic parameters. With regard to the fact that these functions are in conflict with each other in some regions, in this study, three scenarios are considered, each covering three objective functions, and subsequently, three decision making methods are proposed to select the best solutions from three obtained Pareto fronts. The first scenario

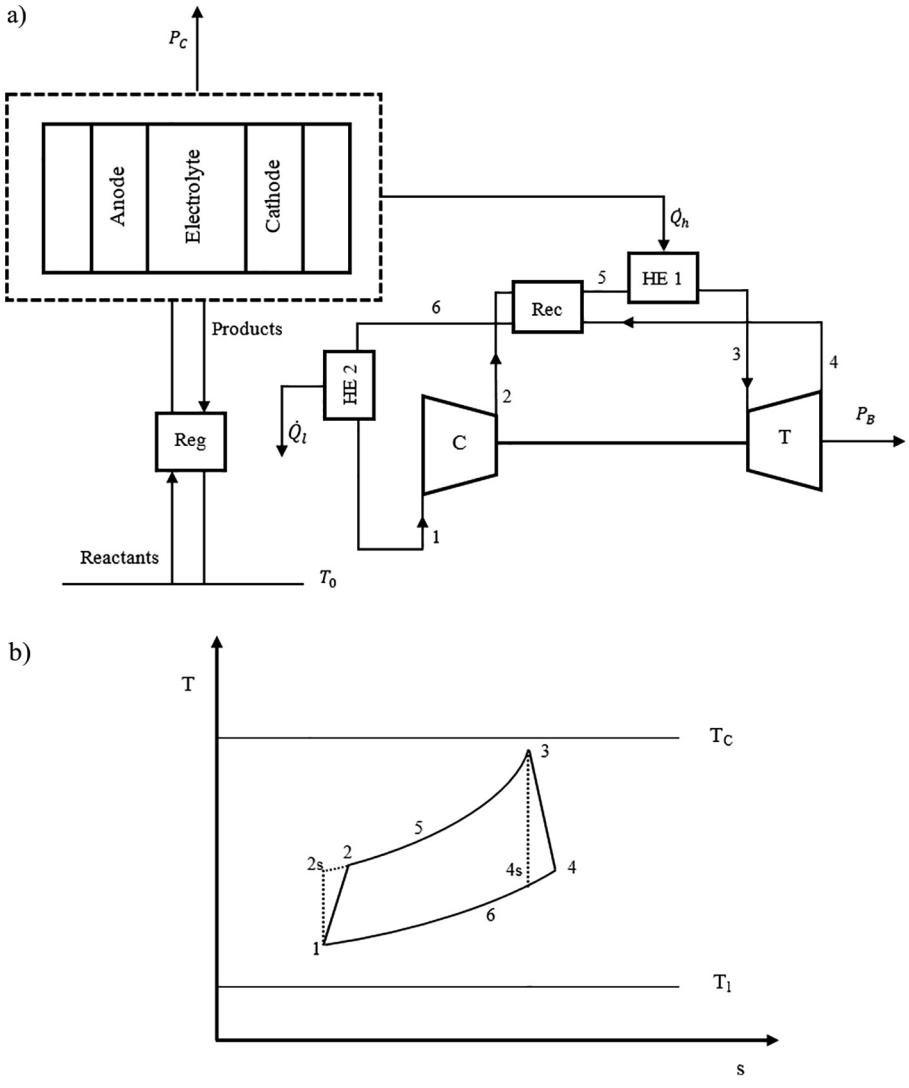

Fig. 1. (a) MCFC - Brayton hybrid heat engine. (b) T-s diagram of Brayton cycle [123].

attempts to maximize energy efficiency and ecological function density, and minimize exergy destruction rate density. The second scenario tries to maximize power density and ecological function density and minimize exergy destruction rate density. The third strategy sets out to maximize energy efficiency and power density and minimize exergy destruction rate density. As a final point, obtained results of the case scenarios are compared to each other.

The obtained decision vectors and the whole procedure can be directly used by designers for developing a better environmentally friendly system. To the authors' knowledge, however, a multi-objective approach like this on MCFC-Brayton hybrid systems was not suggested before. The methodology presented is general and straightforward to carry out in performance optimization of similar systems.

2. Thermodynamic analysis

The system, combination of MCFC and SCO_2 Brayton heat engine, is illustrated in Fig. 1. SCO_2 (point 1) is compressed by the compressor (C) up to turbine inlet pressure (pressure drop in SCO_2 course is neglected). Then, it is preheated in the regenerator and brought into the heat exchanger 1 (point 5). This is where the working fluid of SCO_2 Brayton cycle absorbs heat from MCFC and runs the cycle. The expansion in the gas turbine (process 3–4) supplies mechanical energy and then electricity, in addition to the electricity produced in the MCFC. As aforementioned, the turbine outlet steam (point 4) is used to preheat the SCO_2 flow and then, rejects the low-temperature thermal energy in the heat exchanger 2. The added regenerator where reactants and products of the MCFC are exchanging heat can boost the efficiency of the cycle. For the sake of simplicity, further details and the principle of operation aren't included but they can be found in Refs. [1,3,13,16,18,31,35,38,108,123].

Anode potential (U_{an}), cathode potential (U_{cat}), ohm over-potential (U_{ohm}) and theoretical maximum potential (U_t) of MCFC can be calculated as follows, respectively [123]:

$$U_{an} = 2.27 \times 10^{-9} je^{\left(\frac{En_{act,an}}{RT}\right)} p_{H_2,an}^{-0.42} p_{CO_2,an}^{-0.17} p_{H_2O,an}^{-1} \quad (1)$$

$$U_{cat} = 7.505 \times 10^{-10} je^{\left(\frac{En_{act,cat}}{RT}\right)} p_{O_2,cat}^{-0.43} p_{CO_2,cat}^{-0.09} \quad (2)$$

$$U_{ohm} = 0.5 \times 10^{-4} je^{\left(3016\left(\frac{1}{T}-\frac{1}{923}\right)\right)} \quad (3)$$

$$U_t = U_i + \frac{RT}{n_e F} ln\left(\frac{p_{H_2,an}\,(p_{O_2,cat})^{0.5} p_{CO_2,cat}}{p_{H_2O,an} p_{CO_2,an}}\right) \quad (4)$$

where j is the current density, $p_{H_2,an}$ is partial pressure of hydrogen at the anode, $p_{CO_2,an}$ is partial pressure of carbon dioxide at the anode, $p_{H_2O,an}$ is partial pressure of water at the anode, $p_{O_2,cat}$ is partial pressure of oxygen at the cathode, $p_{CO_2,cat}$ is partial pressure of carbon dioxide at

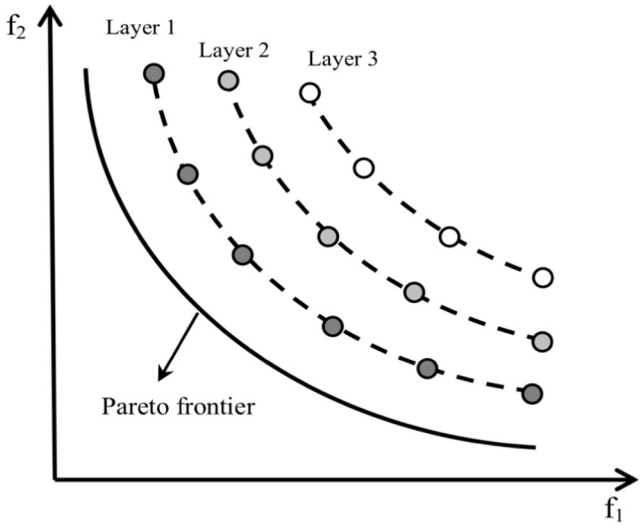

Fig. 3. Solution layering in NSGA-II method.

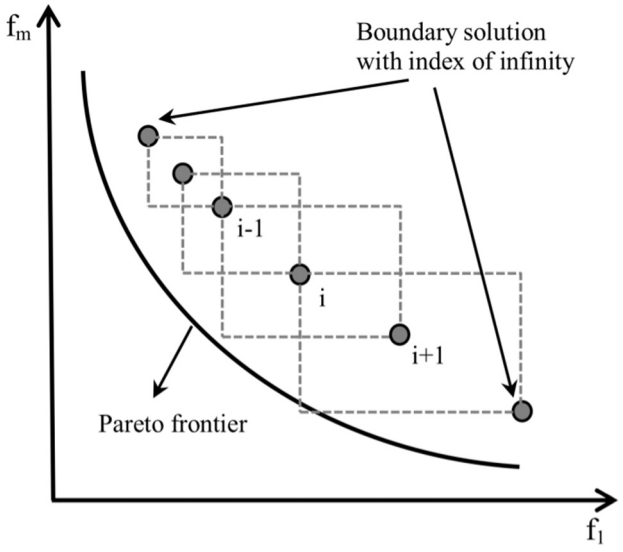

Fig. 4. Distance indexing of each answer in NSGA-II method.

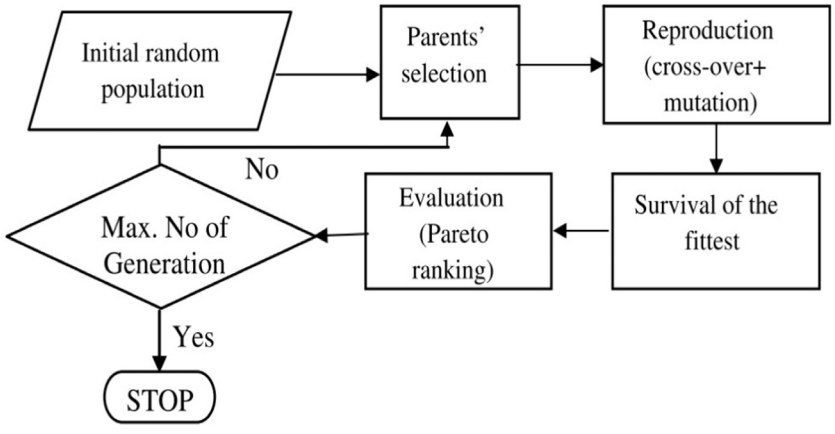

Fig. 2. MOEA approach used in this study.

Table 1
Ranges of the variables used to study their effects on the objectives.

Variable	Compressor inlet temperature (T_1)	Turbine inlet temperature (T_3)	Interconnect plate area (A)	Current density (j)
Unit	K	K	m^2	A/m^2
Lower bound	350	898	0.1	500
Upper bound	400	913	50	6000

Table 2
Specification of GA for optimization puzzle in this paper.

GA parameters	Value
Population size	400
Population type	Double vector
Tournament size	20
Selection process	Tournament
Maximum number of generations	1000
Mutation	Restriction dependent

Table 3
Values of the parameters used in this simulation.

Parameter	Unit	Value
$P_{H_2,an}$, $P_{CO_2,an}$, $P_{H_2O,an}$	atm	0.6, 0.058, 0.342
$P_{O_2,cat}$, $P_{CO_2,cat}$	atm	0.08, 0.08
$En_{act,an}$	J/mol^2	53,500
$En_{act,cat}$	J/mol^2	77,300
R	J/mol·K	8.314
T	K	923
F	C/mol	96,485
n_e	–	2
Δg^0	J/mol	−197,000
Δh	J/mol	−247,430
K_r	W/m^2·K	10
ε_r	–	0.85
T_0	K	298.15
ε_h	–	0.95
ε_{rc}	–	0.98
η_{cp}	–	0.91
η_{ex}	–	0.94
T_l	K	300

the cathode, R is the universal gas constant, T is the operating temperature of the MCFC, En_{act} is the activation energy, F is the Faraday constant, n_e is the number of electrons and U_i is the ideal standard potential.

$$U_i = \frac{-\Delta g^0}{n_e F} \tag{5}$$

Cell voltage is written by using Eqs. (1)–(5):

$$U_{cell} = (U_t - U_{an} - U_{cat} - U_{ohm}) \tag{6}$$

Power and efficiency of the fuel cell are:

$$P_C = U_{cell} jA \tag{7}$$

$$\eta_C = \frac{P_C}{-\Delta \dot{H}} \tag{8}$$

where $-\Delta \dot{H}$ is the maximum possible power from the fuel cell and it can be described as:

$$-\Delta \dot{H} = -\frac{jA\Delta h}{n_e F} \tag{9}$$

where A is area of the interconnect plate and Δh is the molar enthalpy change. Exergy destruction rate of fuel cell is:

$$Exd_C = \left(-\frac{\Delta h}{n_e F} - U_{cell}\right) jA \tag{10}$$

Heat exchange at the regenerator can be described as:

$$\dot{Q}_r = K_r(1-\varepsilon_r)(T - T_0) \tag{11}$$

where K_r is heat conductance of the regenerator, ε_r is the regenerator efficiency and T_0 is the environment temperature. Heat input to the bottom cycle is written as Eq. (12):

$$\dot{Q}_h = -\Delta \dot{H} - P_C - \dot{Q}_r \tag{12}$$

Another heat input expression to the bottom cycle is shown in Eq. (13):

$$\dot{Q}_h = C\varepsilon_h(T - T_5) = C(T_3 - T_5) \tag{13}$$

where C is the heat capacity and ε_h is the effectiveness. T_2 and T_4 temperatures can be calculated by using compression (η_{cp}) and expansion (η_{ex}) efficiencies.

$$\eta_{cp} = \frac{T_{2s} - T_1}{T_2 - T_1},\ \eta_{ex} = \frac{T_3 - T_4}{T_3 - T_{4s}},\left(\frac{T_{2s}}{T_1}\right) = \left(\frac{T_3}{T_{4s}}\right) = x = \left(\frac{p_2}{p_1}\right)^{\frac{k-1}{k}} \tag{14}$$

$$T_2 = \frac{T_{2s} - T_1}{\eta_{cp}} + T_1 \tag{15}$$

$$T_4 = T_3 - \eta_{ex}(T_3 - T_{4s}) \tag{16}$$

where k is the ratio of specific heats and x is the isentropic temperature. T_3, T_5 and T_6 are expressed in Eqs. (17)–(19):

$$T_3 = T_5(1-\varepsilon_{rc}) + \varepsilon_h T \tag{17}$$

$$T_5 = T_2(1-\varepsilon_{rc}) + \varepsilon_{rc} T_4 \tag{18}$$

$$T_6 = T_4(1-\varepsilon_{rc}) + \varepsilon_{rc} T_2 \tag{19}$$

For making easier of the calculations, a correlation between x and j

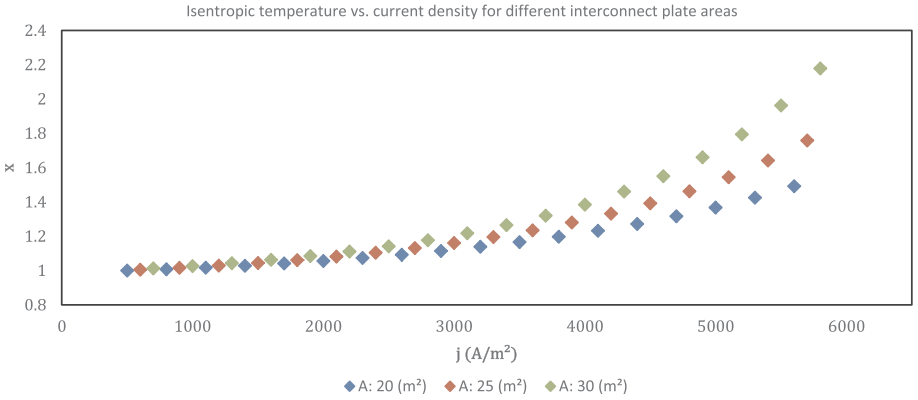

Fig. 5. Isentropic temperature variation with current density for T1: 375 K.

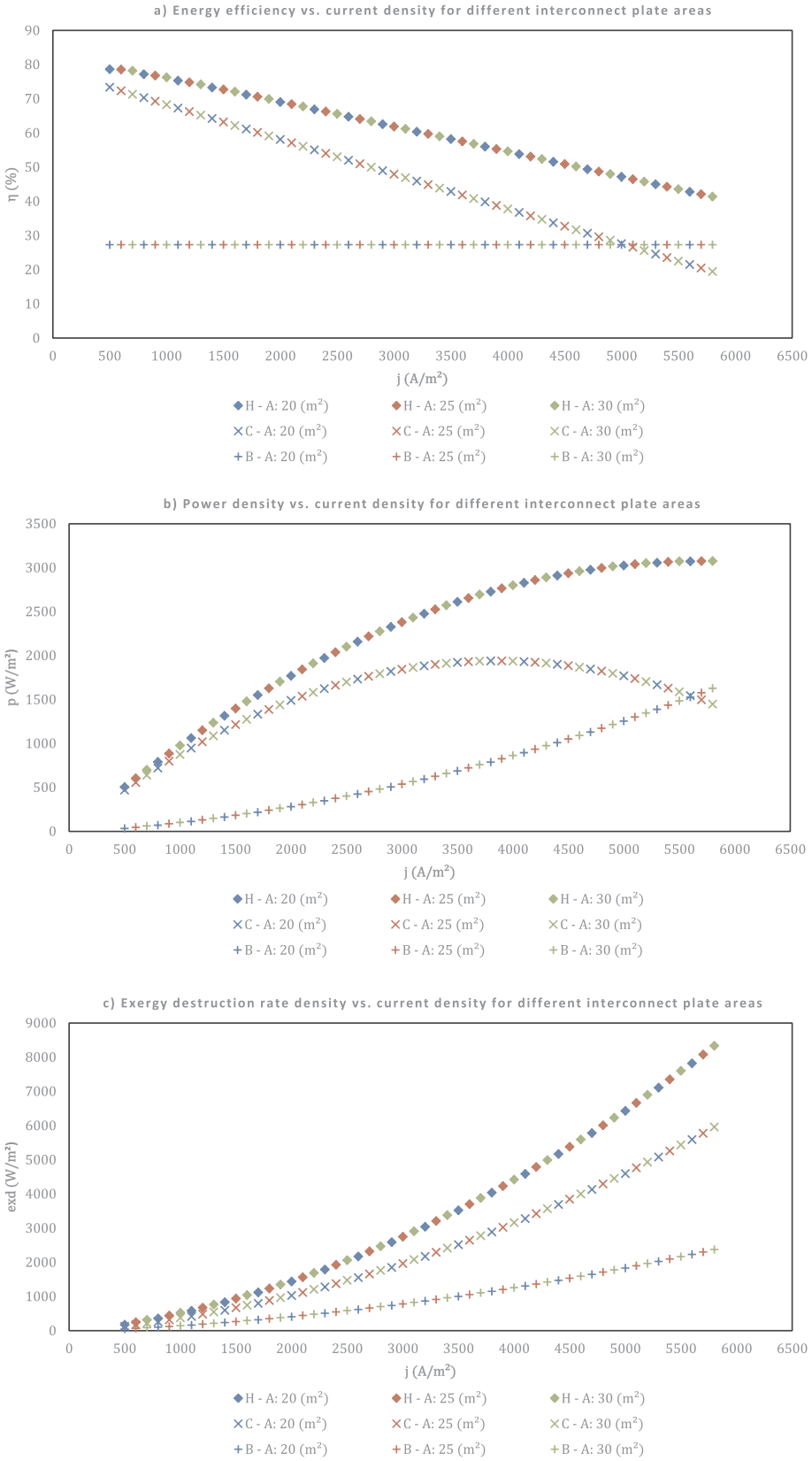

Fig. 6. The influence of the interconnect plate area (A) on the objective functions for T1: 375 K and T3: 908 K (a) Energy efficiency (η), (b) Power density (p), (c) Exergy destruction rate density (exd), and (d) Ecological function density (e).

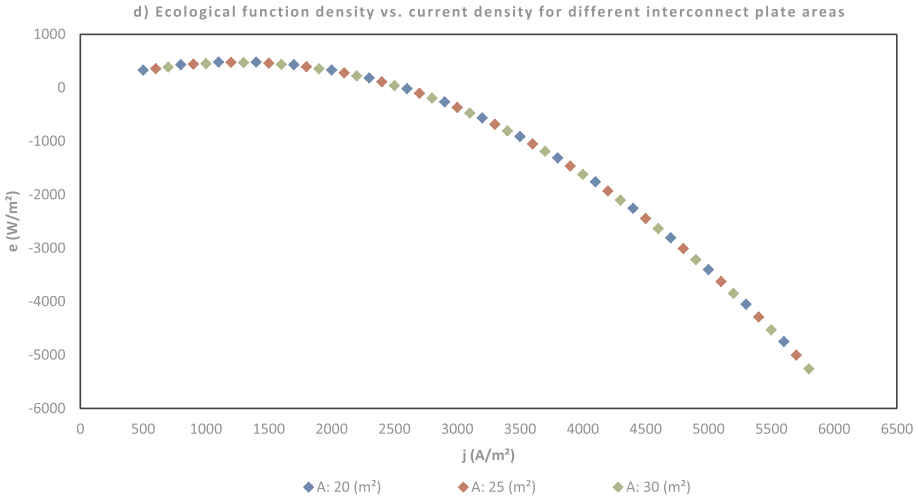

Fig. 6. (*continued*)

can be obtained by using Eqs. (12), (13) and (17) (This correlation is plotted in Fig. 5).

Energy efficiency of the Brayton cycle, under assumption of constant specific heats, is written as following:

$$\eta_B = 1-\frac{\dot{Q}_l}{\dot{Q}_h} = 1-\frac{T_6-T_1}{T_3-T_5} \tag{20}$$

Heat rejection from the Brayton engine is:

$$\dot{Q}_l = \dot{Q}_h(1-\eta_B) \tag{21}$$

Power output of the Brayton cycle is:

$$P_B = \dot{Q}_h-\dot{Q}_l \tag{22}$$

Exergy destruction rate of the Brayton engine is:

$$Exd_B = T_0\left(\frac{\dot{Q}_l}{T_l}-\frac{\dot{Q}_h}{T}\right) \tag{23}$$

Power output, energy efficiency, and exergy destruction rate of the hybrid system are described in Eqs. (24)–(26) respectively.

$$P_H = P_C + P_B \tag{24}$$

$$\eta_H = \frac{P_C + P_B}{-\Delta\dot{H}} \tag{25}$$

$$Exd_H = Exd_C + Exd_B \tag{26}$$

After the basic thermodynamic parameters, environmental criteria may be explained. Ecological function is difference of power output and exergy destruction originated from the entropy generation. It provides an opportunity to maximize power output while reducing exergy destruction and this causes to decrease in the environmental impact of the researched system:

$$E_H = P_H-Exd_H \tag{27}$$

In this paper, power density, the ecological function density and the exergy destruction rate density are introduced as following:

$$p = \frac{P_H}{A} \tag{28}$$

$$e = \frac{E_H}{A} \tag{29}$$

$$exd = \frac{Exd_H}{A} \tag{30}$$

3. Multi-objective optimization with evolutionary algorithms

3.1. Optimization via EA

Genetic Algorithms were introduced by Prof. Holland (1960) by the idea of Darwinian theorem for optimization goals [124]. The evolution normally begins from a society of randomly created individuals and occurs in creations. In each creation, the fitness value of each individual is studied; numerous individuals are randomly selected from the present population and developed to create a fresh population in order to follow the iteration of the GA. Generally, the GA ends when it reaches the termination indexes. More details of GA is presented in the earlier studies [97,105,111,125,126].

Moreover, MOEAs were developed in the recent years by many studies and have present that they can eliminate the difficulties of common approaches. The structure of the MOEA employed in the present study is shown in Fig. 2 [36,89–117,119,120].

3.2. NSGA-II approach

NSGA-II method [36,91,104,107–115,117,119,120] was used in this study with the goal of obtaining the Pareto frontier by running GA. For this reason, NSGA-II organized the answers based on the Pareto theory and arranging non-dominated answers into non-dominated layers as depicted in Fig. 3. In other words, the population number N_p, is classified into N_L layers in which juncture of each two random chosen layer is blank assortment and combination of all layers represents N_p assortment.

Answers virtual fitnesses are related to their layers. For parent selection among two random layers, Tournament selection was employed. Index of crowding distance set the uniform distribution of answers beside layers. This principle is determined as a ratio of undesirability of objective functions for two neighbor answers adjacent the current answer to the undesirability of the extremum amounts of that objective. Therefore, for k_{th} objective of j_{th} answer, we have:

$$i_{dis,j,k} = \frac{f_{k,j-1}-f_{k,j+1}}{f_{k,\max}-f_{k,\min}} \tag{31}$$

For margin, answers are assigned to an unlimited distance index. The sum of individual distances results the overall cumulative distance as follows:

$$I_{dis,j} = \sum_{k=1}^{M} i_{dis,j,k} \tag{32}$$

In which j is the individual index and M is the number of objectives.

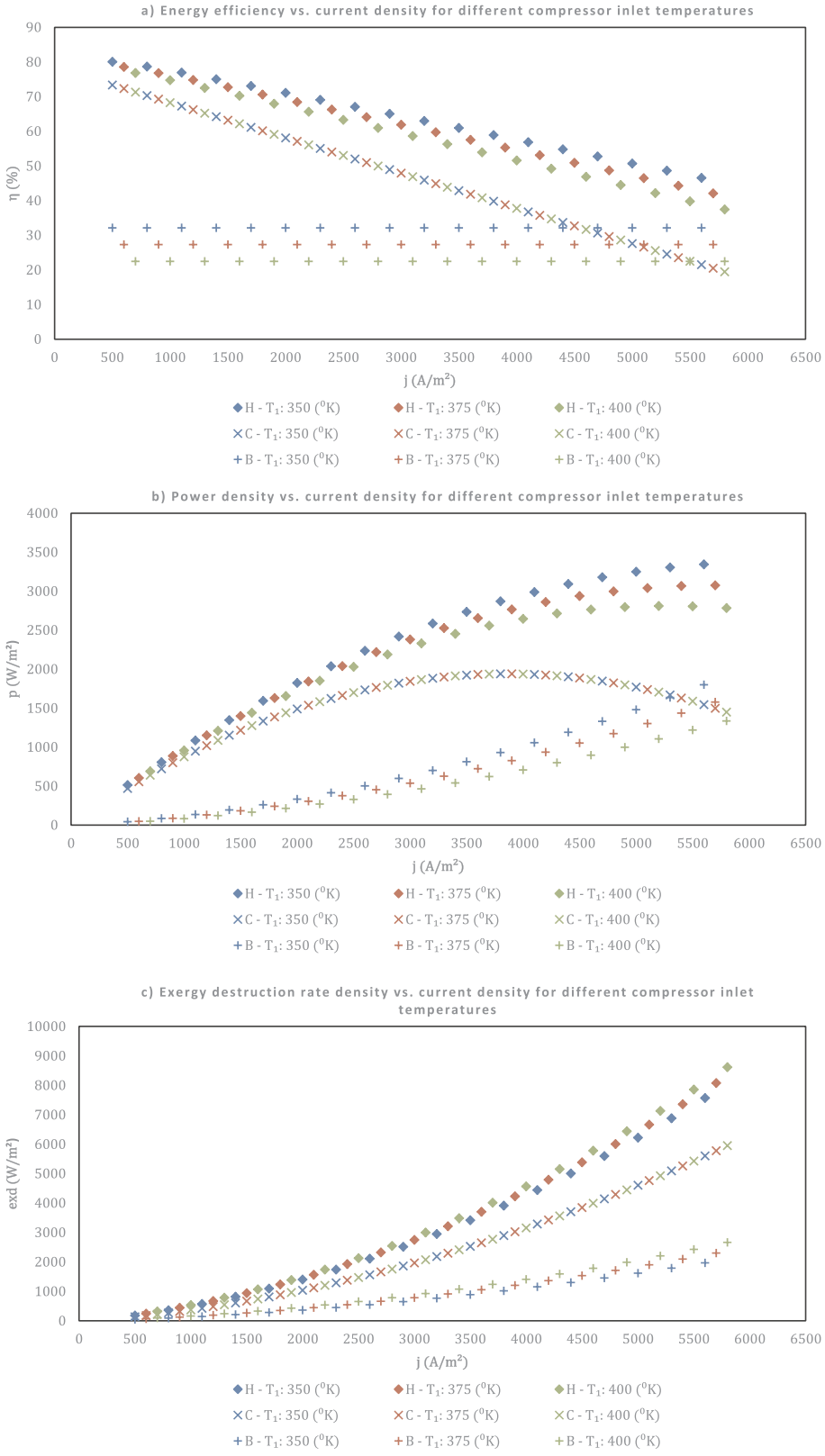

Fig. 7. The influence of the compressor inlet temperature (T1) on the objective functions for A: 25 m^2 and T3: 908 K (a) Energy efficiency (η), (b) Power density (p), (c) Exergy destruction rate density (exd), and (d) Ecological function density (e).

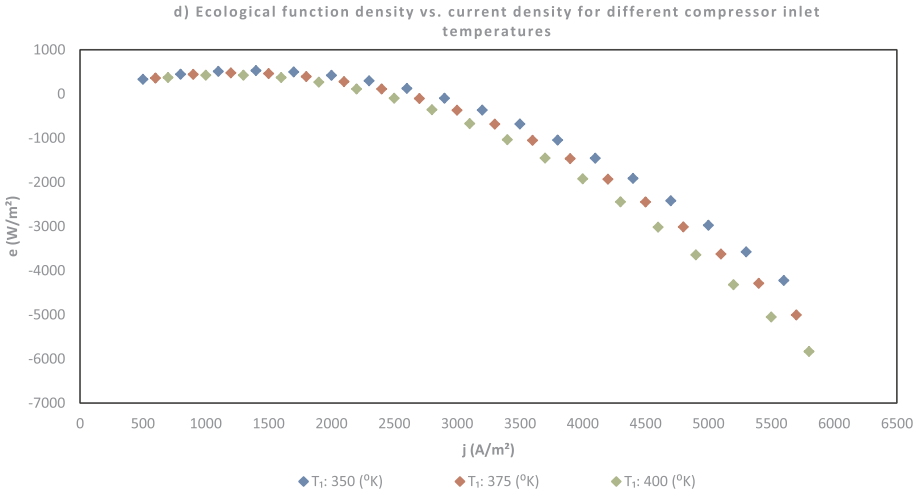

Fig. 7. (*continued*)

Fig. 4 shows a diagram distance indexing. In this method, two variables are set for each answer:

(1) Dominant (Layer) number, N_L, which is the number of answers that control the current answer. More explanations of domination were presented in Refs. [86,87]. Dominant number, for non-dominated answers of the existing population is 0. Thus, these answers are set in layer 1. Non-dominated answers which do not include the layer 1 numbers, are located in layer 2. There would be MN^2 assessments for M objectives and N populations. This routine continued with the goal of accepting all answers in their appropriate layers. Moreover, i rank indexes of answers are assigned to their layer number, N_L.
(2) Crowded comparison operator, n≺, is presented as:

$$\begin{aligned} &A \prec \text{Bif}(\text{rank}_A < rank_B) \\ &\text{Or:} \\ &((\text{rank}_A = \text{rank}_B) \text{ and } I_{dis,A} > I_{dis,B}) \end{aligned} \tag{33}$$

It shows that for answers with different layers, the answer with the minor layer is preferred. On the other hand, for identical layer answers, the answer of lower concentration area is selected.

3.3. Objective functions, restraints and decision variables

Table 1 shows the ranges of the decision variables used for this optimization which are determined by the suggestions provided in the literature [35,108,114,123].

Energy efficiency, ecological function density and exergy destruction rate density are the three objective functions for the first scenario evaluated via Eqs. (25), (29) and (30).

Power density, ecological function density and exergy destruction rate density are the three objective functions for the second scenario evaluated via Eqs. (28)–(30).

Energy efficiency, power density, and exergy destruction rate density are the three objective functions for the third scenario evaluated via Eqs. (25), (28) and (30).

To determine the optimal design variables of the system based on genetic algorithm approach, a simulation program was coded through Matlab software [127], due to the complexity of the problem. Details of the developed program is beyond the scope of this paper. Specifications of GA for optimization puzzle are reported in Table 2.

3.4. Decision-making in the multi-objective optimization

In order to pick up the best solution of Pareto optimal frontier, decision making tools should be employed. Hence, three expert decision maker methods: Fuzzy, TOPSIS and LINMAP are utilized.

3.4.1. Non-dimensionalization methods

3.4.1.1. Euclidean non-dimensionalization. F_{ij}^n is the matrix of objectives for various solutions of the Pareto frontier and i is the index of each solution, and j presents the index of the objective in the objective area. A non-dimensioned objective, F_{ij}^n, is defined as follows.

$$F_{ij}^n = \frac{F_{ij}}{\sqrt{\sum_{i=1}^{m} (F_{ij})^2}} \quad \text{aimed at extremum goals} \tag{34}$$

3.4.1.2. Fuzzy non-dimensionalization. A non-dimensioned objective, F_{ij}^n, is defined as follows:

$$F_{ij}^n = \frac{F_{ij} - \min(F_{ij})}{\max(F_{ij}) - \min(F_{ij})} \quad \text{for maximizing.} \tag{35a}$$

$$F_{ij}^n = \frac{\max(F_{ij}) - F_{ij}}{\max(F_{ij}) - \min(F_{ij})} \quad \text{for minimizing.} \tag{35b}$$

The fuzzy non-dimensionalization technique is used in the Bellman-Zadeh approach; while, Euclidean non-dimensionalization technique is used in TOPSIS and LINMAP approaches.

3.4.2. Decision-making methods

The decision making methods are briefly introduced below. However, they are described in greater detail in the earlier studies [92–95,98,105].

3.4.2.1. Bellman-Zadeh decision-making method. The final solution, maximum value of the lowest membership function of objectives, in this method is obtained based on relations of all fuzzy criteria and restrictions and the related membership function.

3.4.2.2. LINMAP decision-making method. In LINMAP approach, the final solution is selected based on ideal point, which is defined as the point on the Pareto frontier where each objective is optimized disregarding counting the other objectives. In LINMAP, the optimum solution is obtained based on the shortest distance in space from the ideal data point.

3.4.2.3. TOPSIS decision-making method. In TOPSIS approach for finding the best solution, another index called “non-ideal point” should be obtained first. Non-ideal point is defined as the point where each objective has its worst value. Afterwards, the final

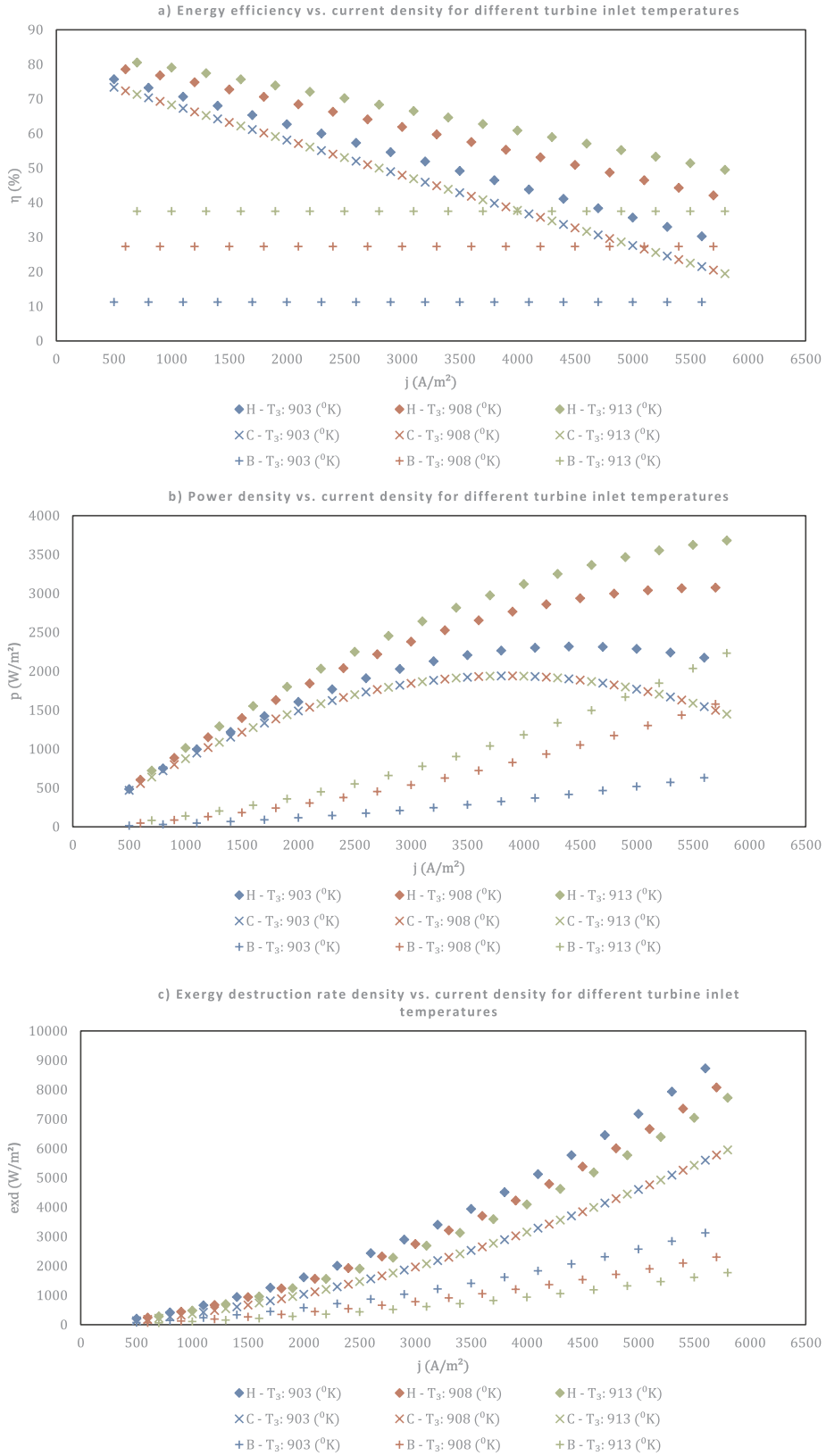

Fig. 8. The influence of the turbine inlet temperature (T3) on the objective functions for A: 25 m^2 and T1: 375 K. (a) Energy efficiency (η), (b) Power density (p), (c) Exergy destruction rate density (exd), and (d) Ecological function density (e).

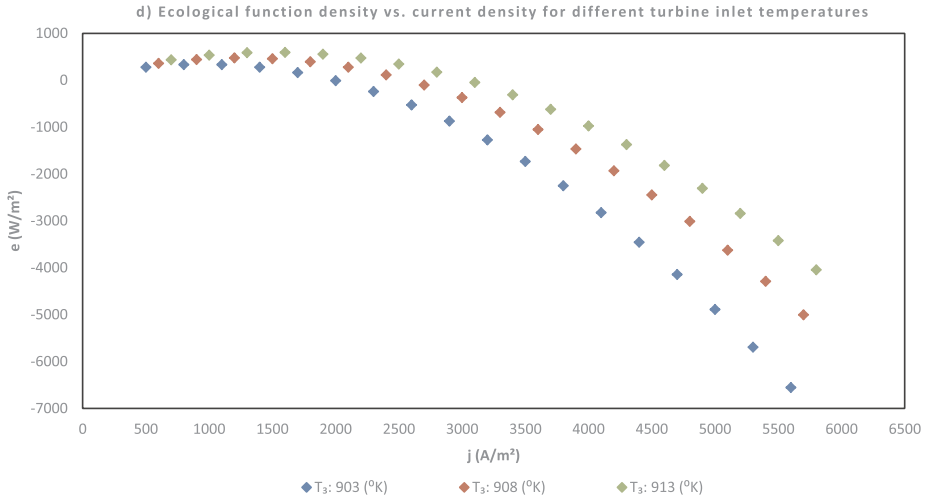

Fig. 8. (*continued*)

solution in the TOPSIS approach is selected based on the shortest distance from the ideal point and highest distance from the non-ideal point, concurrently.

4. Results and discussion

4.1. Simulation results and sensitivity analysis

In this simulation four objective functions are considered to be optimized including: energy efficiency (η_H), power density (p), exergy destruction rate density (exd) and ecological function density (e), and four variables changed to study their effects on these targets including: current density (j), interconnect plate area of the fuel cell (A), compressor inlet temperature (T_1) and turbine inlet temperature (T_3). Parameters used for this simulation are listed in Table 3. The performance characteristic curves are plotted in Figs. 6–8, each consists of four figures, and the coordinates of some important points on the curves are demonstrated in Fig. 9(a–d) by which the influence of the main parameters can be quantitatively investigated. Before these curves, the following is Fig. 5 which shows isentropic temperature (x) variation with current density (j). This parameter governs the thermodynamics of the Brayton cycle because directly determines the compressor pressure ratio.

Current density is a very crucial parameter and its variation enormously influences all targets, corresponding to its nature which defines the operating condition of the whole system. Therefore it is considered as the basic variable (the horizontal axis) in studying the effect of other three variables enabling to see its effect on the system specifically. As it was expected, by increasing the current density, power density of the Brayton cycles increases while the energy efficiency of the Brayton cycle does not and stays constant. This increase, which is more than a linear one, clearly happens due to the fact that the more energy the Brayton cycle receives from the fuel cell, the more energy there is to be converted to power as the current density increases. Moreover, in this situation, the heat rejected from the fuel cell to the environment ($\dot{Q}_r$) is fixed, because it isn't a function of the current density, and the energy efficiency of the Bryton cycle remains constant, because it is only a function of the features of the Brayton cycle. Therefrom there should be, as there is, more than a linear increase in the power density of the Brayton cycle.

The linear relation between the energy efficiency of the fuel cell and the current density corresponds to the linear relation between the cell voltage and the current density (Eqs. (1)–(6)). It should be noted that the theoretical maximum potential of the fuel cell (U_t) determines the point where the curve starts and also explains the fact that the maximum energy efficiency of the hybrid cycle is occurred at the small values of the current density.

The interconnect plate area (A) is another important parameter which defines the size of the fuel cell system and therefore all targets were generally defined as their value per unit area of the interconnect plate. By fixing other three variables, j, T_1, and T_3, the efficiency of the Brayton cycle is determined and also the efficiency of the fuel cell system, and changing this parameter doesn't affect that, due to given parameters which determine the amount of heat that rejects from MCFC ($\dot{Q}_r$). Eqs. (6)–(9) and (12)–(20) show how this happens. Power density and exergy destruction rate is not influenced by A; and this is the same for ecological function which is their differences. Fig. 6a–d as well show there are no meaningful variations of the targets (energy efficiency, power density, exergy destruction rate density and ecological function density) with A. These figures also show how the region of the current density (500–6000 A/m^2) was selected for the investigation. By increasing the current density, before $j = 500$ (A/m^2) the energy efficiency is increasing until it approaches its maximum, somewhere after this point, and then decreases. On the other hand, the power density is increasing along with increase in the current density in this region and attains its maximum before $j = 6000$ (A/m^2). Besides, the ecological function maximization occurs within this region, too. Therefore the optimal current density should be situated in this region.

The variations of the targets with the compressor inlet temperature is illustrated in Fig. 7(a–d). By increasing the compressor inlet temperature, energy efficiency and power density of the Brayton cycle decreases. The reason can be expounded as follows: when A is kept as a constant, the heat the Brayton cycle receives from the fuel cell ($\dot{Q}_h$) is constant, too, which also results into a constant C and T_5, according to Eq. (13). Consequently, according to Eqs. (12)–(20), by increasing the compressor inlet temperature, the heat amount that has to be rejected from the cycle ($\dot{Q}_l$) is increased, and therefore energy efficiency and power density are decreased. In this situation, exergy destruction rate density increases, according to Eq. (23), leading to the less ecological function.

The opposite behavior is followed when the compressor inlet temperature is kept as a constant and the turbine inlet temperature

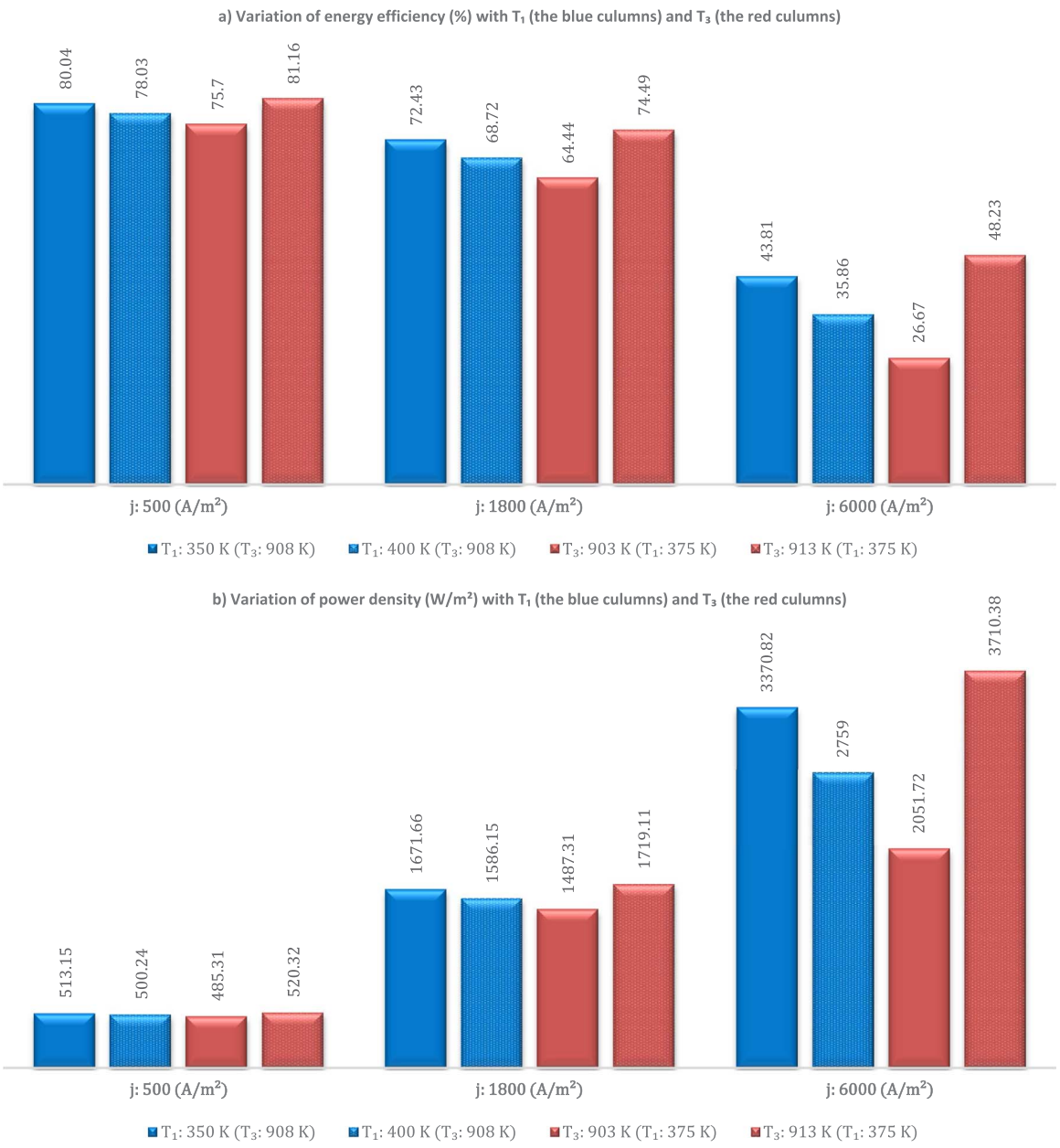

Fig. 9. The impact of the compressor inlet temperature (T1) and the turbine inlet temperature (T3) on the objective functions of the hybrid system for A: 25 (m^2). (a) Energy efficiency (ηH), (b) Power density (p), (c) Exergy destruction rate density (exd), and (d) Ecological function density (e).

increases, as Fig. 8(a–d) show. The more the turbine inlet temperature, the more energy efficiency, power density and ecological function density, and also the less exergy destruction rate density. This behavior can be expounded as follows: when A is kept as a constant, the heat the Brayton cycle receives from the fuel cell ($\dot{Q}_h$) is again constant. But by fixing the inlet temperature of the compressor, more work is needed by the compressor and also more work is produced by the turbine, clearly obvious in the T-s diagram of the Brayton cycle. Because the turbine works in a higher temperature, its work increases more than that of the compressor within the same pressures. Therefore, energy efficiency increases and also net power density. The reduction of exergy destruction rate density can also be realized here, with respect to Eqs. (20)–(23).

It can be found from Figs. 6–8 d that ecological function density first increases and then decreases as the current density is increased for any given interconnect plate area or compressor inlet temperature or turbine inlet temperature. This maximum point is approximately considered at $j = 1800$ (A/m^2) for further studies. This point and other two main points including $j = 500$ (A/m^2), where the curves start, and $j = 6000$ (A/m^2), where the curves end, were selected and the objectives were calculated at these points. The results are depicted in Fig. 9(a–d). Then the sensitivity of each objective to both T_1 and T_3 are computed.

The sensitivity of the objective functions to the compressor inlet temperature is as follows, according to Fig. 9(a–d): By a change of 14.29% in the compressor inlet temperature (from 350 to 400 K), energy efficiency varies −2.51%, −5.12%, and −18.15%, at $j = 500$,

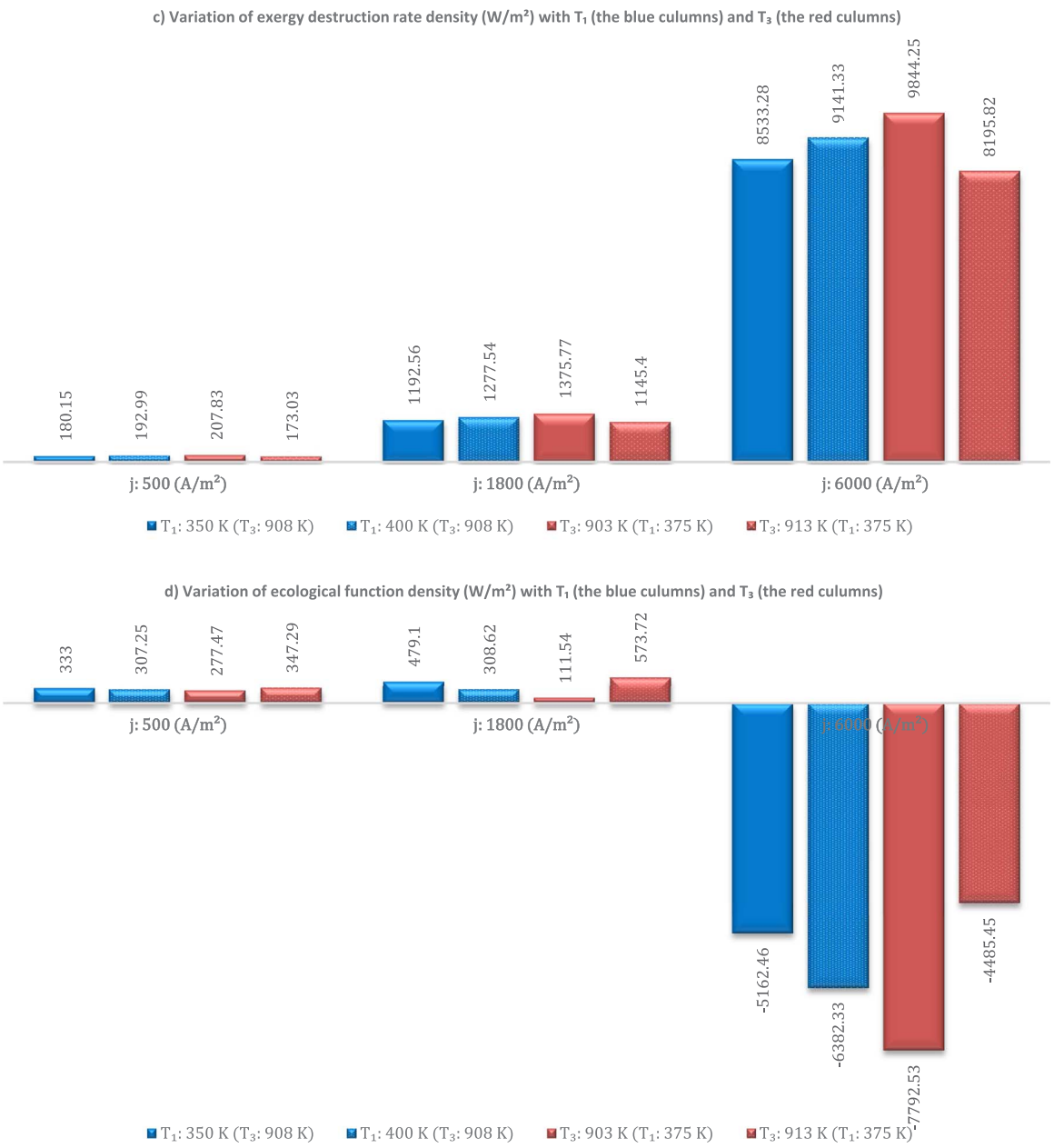

Fig. 9. (*continued*)

1800, and 6000 (A/m^2) respectively; power density similarly varies −2.52%, −5.12%, and −18.15%, while exergy destruction rate density varies 7.13%, in all three situations, and ecological function density varies −7.73%, −35.58%, and −23.63%. And the sensitivity of the objective functions to the turbine inlet temperature is as follows: By a change of 1.11% in the turbine inlet temperature (from 903 to 913 K), energy efficiency varies 7.21%, 15.6%, and 80.84%, at j=500, 1800, and 6000 (A/m^2) respectively; in the same way power density varies 7.21%, 15.59%, and 80.84%, while exergy destruction rate density varies −16.75%, again in all three situations, and finally, ecological function density varies 25.16%, 414.36%, and 42.44%.

These results show that energy efficiency and power density are equally influenced by changing T_1, or T_3. This can be explained referring to Eqs. (20)–(22), which show both the energy efficiency and the power density of the Brayton cycle are similarly dependent on four important temperatures of the cycle (T_1, T_3, T_5, and T_6). The difference is that the power density is also influenced by the heat the Brayton cycle receives from the fuel cell ($\dot{Q}_h$), which is not a function of T_1, or T_3. Hence, dependencies of these functions on T_1 and T_3 are the same (but their dependencies on j can still be seen in the figures). Moreover, the fuel cell energy efficiency and power density are clearly not functions of T_1, or T_3, as the figures demonstrate, too. Therefore the energy efficiency and the power density of the hybrid system are also equally influenced by changing in T_1, or T_3.

Another point can be seen in these figures is that the sensitivity of the exergy destruction rate density of the hybrid cycle to T_1, or T_3, doesn't change by varying the current density (j). This may be explained as by referring to Eqs. (10), (12) and (20)–(23) which show that when a

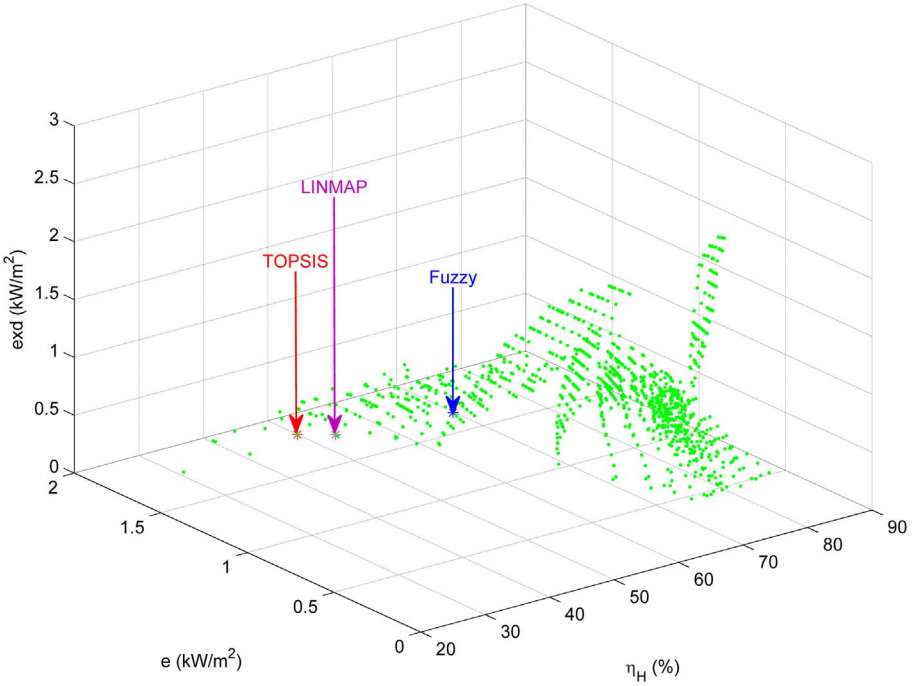

Fig. 10. Pareto optimal frontier in the objectives' space for the first scenario.

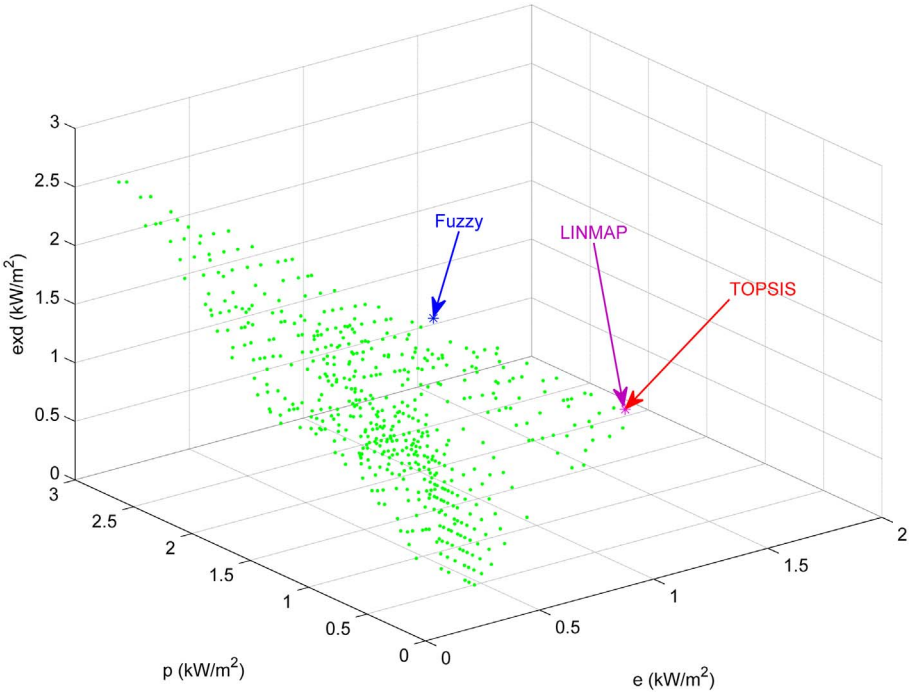

Fig. 11. Pareto optimal frontier in the objectives' space for the second scenario.

set of the important temperatures of the Brayton cycle (T_1, T_3, T_5, and T_6) are given, current density variation just affects the heat amount the Brayton cycle receives from the fuel cell ($\dot{Q}_h$), and equally, the heat amount it rejects to the environment ($\dot{Q}_l$). In other words, there is the same dependency between j and $\dot{Q}_h$, and between j and $\dot{Q}_l$, which leads to the same dependency between j and exd_B. Therefrom, with respect to the relation between the exergy destruction rate of the fuel cell and the current density, which is the same as $\dot{Q}_h$, this similarity can be

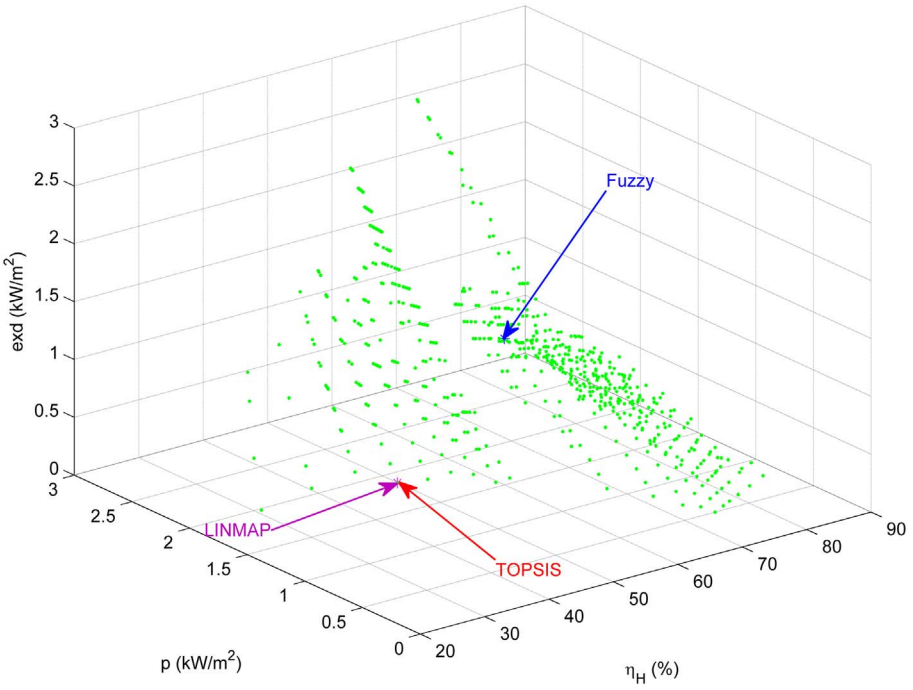

Fig. 12. Pareto optimal frontier in the objectives' space for the third scenario.

Table 4
Outcomes of the decision makers for the first scenario.

Decision making method	Decision variables				Considered objective functions			Not-considered objective function
	A (m^2)	j (A/m^2)	T_1 (K)	T_3 (K)	η_H (%)	e (kW/m^2)	exd (kW/m^2)	p (kW/m^2)
TOPSIS	0.5	2900	350	913	49.22	1.8006	0.0296	1.8301
LINMAP	0.6	2600	350	913	52.48	1.7018	0.0477	1.7494
Fuzzy	1	2200	359	912.5	60.28	1.3140	0.3864	1.7004
Ideal point	–	–	–	–	83.19	1.8804	0.0184	2.2886
Non-ideal point	–	–	–	–	23.81	0.0004	2.6675	0.0013

Table 5
Outcomes of the decision makers for the second scenario.

Decision making method	Decision variables				Considered objective functions			Not-considered objective function
	A (m^2)	j (A/m^2)	T_1 (K)	T_3 (K)	e (kW/m^2)	p (kW/m^2)	exd (kW/m^2)	η_H (%)
TOPSIS	0.3	4000	350	912.8	1.8800	1.9650	0.0850	38.32
LINMAP	0.3	4000	350	912.8	1.8800	1.9650	0.0850	38.32
FUZZY	0.4	4000	353	912.5	1.1999	2.2783	1.0785	44.42
Ideal point	–	–	–	–	1.8804	2.2886	0.0184	83.19
Non-ideal point	–	–	–	–	0.0004	0.0013	2.6675	23.81

Table 6
Outcomes of the decision makers for the third scenario.

Decision making method	Decision variables				Considered objective functions			Not-considered objective function
	A (m^2)	j (A/m^2)	T_1 (K)	T_3 (K)	P (kW/m^2)	η_H (%)	exd (kW/m^2)	e (kW/m^2)
TOPSIS	0.5	2900	350	913	1.8301	49.22	0.0296	1.8005
LINMAP	0.5	2900	350	913	1.8301	49.22	0.0296	1.8005
FUZZY	2	2200	358	912.3	1.8833	66.76	0.9876	0.8957
Ideal point	–	–	–	–	2.2886	83.19	0.0184	1.8804
Non-ideal point	–	–	–	–	0.0013	23.81	2.6675	0.0004

corroborated. In brief, exergy destruction rate density of the hybrid system is proportional to the second order of the current density.

Additionally, another conclusion from Fig. 9(a–d) is that the sensitivity of ecological function to the variation of T_1, or T_3, is at its maximum where ecological function is also approaching to its maximum. This point shows how important it is to adjust exactly the optimum concrete values of T_1 and T_3 for obtaining the maximum possible ecological function density. It is also evident that the sensitivity of energy efficiency and power density to T_1, or T_3, rises by the increase in the current density. So, when one wants to optimize power density, which leads to high values of current density, the optimization of T_1, or T_3, becomes more substantial.

Finally, it is also should be pointed out that, as it seems natural, the sensitivity of objectives to the turbine inlet temperature is greater than that of the compressor. As it mentioned earlier, the maximum temperature of the hybrid cycle, which is the operating temperature of the fuel cell (T), confines this essential parameter of the Brayton cycle. Therefore, by increasing this parameter, which corresponds to some special issues such as the investment cost, the technical issues due to the required thermal stability of the cell and other operating limitations, the ecological function density of the hybrid system improves.

4.2. Optimization results

It should be mentioned that there is no combination of the variable values that concurrently optimizes all the objective functions. One of the main results of the parametric evaluation section is that each objective function is optimized in a particular region which can be observed clearer in this section. According to Figs. 6–8, by increasing current density, energy efficiency first increases for a short range and then decreases till the end; ecological function also increases along with the increase in the current density but attains its maximum at larger current densities. Afterwards, ecological function decreases, the same as energy efficiency. Therefore, between the points where energy efficiency is maximum and that of ecological function, there has to be a compromise when one wants to optimize both of them. Exergy destruction rate and power output have similar trends. Both of them approach to their maximum value by increase in current density which makes the concurrently optimization of them more complicated. One can compare influences of current density on the other two pairs of objectives from Figs. 6–8. Other variables, including interconnect plate area, compressor inlet temperature, and turbine inlet temperature, have similar effects on optimizing the objective functions. All objective functions improve by increasing turbine inlet temperature or decreasing compressor inlet temperature, and changing interconnect plate area does not affect their optimums.

The comparison of objective functions at different values of input variables becomes more complicated when one wants to optimize three of them simultaneously. Therefore, after providing the sets of best possible solutions (Pareto fronts) for each scenario, decision-making methods should be applied to obtain the best solutions. In this study, the global optimization toolbox, developed in Matlab, is used with the default settings and parameters in order to implement genetic algorithm to obtain Pareto fronts needed in the next step. Four objectives discussed in the previous section are considered for three multi-objective optimizations: energy efficiency (to be maximized), power density (to be maximized), ecological function density (to be maximized), and exergy destruction rate density (to be minimized); in this manner, three scenarios are considered to investigate the simultaneous optimization and in each scenario three targets are considered. Power density, energy efficiency, and ecological function density are left out and other three objectives are optimized in scenario one, two, and three, respectively. The results are shown in Figs. 10–12. Three ultimate answers are chosen by the LINMAP, Fuzzy, and TOPSIS decision makers highlighted in these figures.

Pareto optimal frontier for case scenario one is represented in Fig. 10 and Table 4 depicts the optimal outputs achieved for objective functions and decision parameters by executing LINMAP, Fuzzy and TOPSIS approaches.

Fig. 11 depicts the Pareto frontier in the suggested objectives' space achieved in the second optimization scenario. Table 5 reports the optimal outputs achieved for the objective functions and decision parameters.

Pareto optimal frontier for case scenario three is represented in Fig. 12 and Table 6 reports the optimal outputs achieved for the objective functions and decision parameters via running TOPSIS, Fuzzy and LINMAP approaches.

From Tables 4–6, as already expected, can be found that the offered points are situated at higher turbine inlet temperatures and lower compressor ones. If the stopping criteria weren't already satisfied, the program would continue running and reach the upper and lower bounds of turbine and compressor inlet temperatures, respectively. Different values suggested for current density, as the most powerful case parameter, are subject to the differences between decision making methods. Finally, lower values of A is because of the fact that in this region, according to the given parameters, the sensitivity of the objective functions to the area is a little more than that of higher values. Therefore, the developed computer model tends to find the Pareto front near this area. Nevertheless, there is only a very little dependency of the objective functions to the area in its whole region. The effect of not considering one objective function in each scenario can also be seen in Tables 4–6. In the conclusions section, however, for the sake of simplicity, only the results of Fuzzy method are reviewed. Other methods can be analyzed in the same way.

5. Conclusions

This paper presents a comprehensive modeling, parametric evaluation, and multi-objective optimization of a hybrid system consisting of a Brayton cycle and a molten carbonate fuel cell. Beginning by a thermodynamic simulation, a study on the effect of main variables of the hybrid cycle, including compressor inlet temperature (T_1), turbine inlet temperature (T_3), interconnect plate area (A), and current density (j), on the objective functions, including energy efficiency (η_H), power density (p), exergy destruction rate density (exd), and ecological function density (e), is carried out. Some important results are reviewed here:

- Energy efficiency maximization and minimization of exergy destruction rate density occur at small values of current density, while power density attain its maximum at higher ones. This makes ecological function optimum value to be situated in a range between these bounds, therefore, also indicating that there is an optimum range for current density rather than a single value.
- After selecting an optimum range of current density, the next most important parameter is turbine inlet temperature whose optimum value should be chosen in conjunction with considering economic criteria. The fuel cell operating temperature (T) and turbine limitations confine this value.
- According to the sensitivity analysis, the dependency of targets on 1.11% variation in the turbine inlet temperature is greater than a change of 14.29% in the compressor inlet temperature.
- Ecological function is more dependent on T_1, and also T_3, when approaches its maximum while those of energy efficiency and power density increase along with the increase in current density.

The purpose of the next step is to develop a comprehensive optimum design procedure for the proposed system. MOEA based on NSGA-II approach is employed to investigate optimization of the decision variables, considering three objectives in each case scenario. The triple-objective optimization algorithm is employed for energy efficiency and ecological function density maximization and exergy

destruction rate minimization as the first scenario. In the second one, instead of energy efficiency, power density is taken as one of the objective functions while the other goals are the same as the first scenario. In the third scenario, the algorithm is applied in order to maximize energy efficiency and power density and minimize exergy destruction rate density. Subsequently, Pareto-optimal frontiers are obtained.

Lastly, for each case scenario three ultimate optimum answers are chosen via three competent decision makers comprising LINMAP, Fuzzy, and TOPSIS approaches. Comparing their results shows which objective function has better condition in each case scenario. Making inferences from the Fuzzy method results, for example, it seems that the first scenario would provide better condition for the system. Ecological function density meets its maximum (1.314 kW/m^2) in this scenario, where power density is not considered, and falls by 9 and 31% in the second and third scenario, respectively. Energy efficiency is at its maximum (0.6676) in the third scenario, where ecological function density is not considered, and reduces by 10 and 33% in the first and second scenario, respectively. Power density reaches its pick (2.2783 kW/m^2) in the second scenario, where energy efficiency is not considered, and drops by 25 and 17% in the first and third scenario, respectively. Exergy destruction rate density is considered in all case scenarios. However, it is at its optimum value (0.3864 kW/m^2) in the first scenario, similar to ecological function density, and increases by 179 and 155% in the second and third scenario, respectively.

To bring the paper to a close, it should be acknowledged that the multidisciplinary approach proposed here still lacks considering other effective parameters of the hybrid cycle and probably other relevant objective functions. However, it can be readily extended to FC-heat engine hybrid systems of any configuration to achieve the optimum performance taking into account a variety of decision variables and objective functions.

References

[1] Zhao Y, Ou C, Chen J. A new analytical approach to model and evaluate the performance of a class of irreversible fuel cells. Int J Hydrogen Energy 2008;33:4161–70.
[2] Zhang X, Guo J, Chen J. The parametric optimum analysis of a proton exchange membrane (PEM) fuel cell and its load matching. Energy 2010;35:5294–9.
[3] Zhang H, Lin G, Chen J. Performance analysis and multi-objective optimization of a new molten carbonate fuel cell system. Int J Hydrogen Energy 2011;36:4015–21.
[4] Zhang H, Lin G, Chen J. Multi-objective optimisation analysis and load matching of a phosphoric acid fuel cell system. Int J Hydrogen Energy 2012;37:3438–46.
[5] Zhang H, Chen L, Zhang J, Chen J. Performance analysis of a direct carbon fuel cell with molten carbonate electrolyte. Energy 2014;68:292–300.
[6] E J, Zhao X, Liu H, Chen J, Zuo W, Peng Q. Field synergy analysis for enhancing heat transfer capability of a novel narrow-tube closed oscillating heat pipe. Appl Energy 2016;175:218–28.
[7] E J, Zuo W, Liu X, Peng Q, Deng Y, Zhu H. Effects of inlet pressure on wall temperature and exergy efficiency of the micro-cylindrical combustor with a step. Appl Energy 2016;175:337–45.
[8] E J, Zuo W, Liu H, Peng Q. Field synergy analysis of the micro-cylindrical combustor with a step. Appl Therm Eng 2016;93:83–9.
[9] Zuo W, E J, Peng Q, Zhao X, Zhang Z. Numerical investigations on thermal performance of a micro-cylindrical combustor with gradually reduced wall thickness. Appl Therm Eng 2017;113:1011–20.
[10] Chen X, Li W, Gong G, Wan Z, Tu Z. Parametric analysis and optimization of PEMFC system for maximum power and efficiency using MOEA/D. Appl Therm Eng 2017;121:400–9.
[11] Haseli Y, Dincer I, Naterer G. Thermodynamic modeling of a gas turbine cycle combined with a solid oxide fuel cell. Int J Hydrogen Energy 2008;33:5811–22.
[12] Haseli Y, Dincer I, Naterer G. Thermodynamic analysis of a combined gas turbine power system with a solid oxide fuel cell through exergy. Thermochim Acta 2008;480:1–9.
[13] Zhao Y, Chen J. Modeling and optimization of a typical fuel cell–heat engine hybrid system and its parametric design criteria. J Power Sources 2009;186:96–103.
[14] Zhang X, Chen J. Performance analysis and parametric optimum criteria of a class of irreversible fuel cell/heat engine hybrid systems. Int J Hydrogen Energy 2010;35:284–93.
[15] Chen X, Chen L, Guo J, Chen J. An available method exploiting the waste heat in a proton exchange membrane fuel cell system. Int J Hydrogen Energy 2011;36:6099–104.
[16] Zhang H, Lin G, Chen J. Performance evaluation and parametric optimum criteria of an irreversible molten carbonate fuel cell-heat engine hybrid system. Int J Electrochem Sci 2011;6:4714–29.
[17] Zhang X, Su S, Chen J, Zhao Y, Brandon N. A new analytical approach to evaluate and optimize the performance of an irreversible solid oxide fuel cell-gas turbine hybrid system. Int J Hydrogen Energy 2011;36:15304–12.
[18] Zhang X, Guo J, Chen J. Influence of multiple irreversible losses on the performance of a molten carbonate fuel cell-gas turbine hybrid system. Int J Hydrogen Energy 2012;37:8664–71.
[19] Zhang H, Su S, Lin G, Chen J. Performance analysis and multi-objective optimization of a molten carbonate fuel cell-Braysson heat engine hybrid system. Int J Electrochem Sci 2012;7:3420–35.
[20] Chen L, Gao S, Zhang H. Performance analysis and multi-objective optimization of an irreversible solid oxide fuel cell-stirling heat engine hybrid system. Int J Electrochem Sci 2013;8:10772–87.
[21] Chen L, Zhang H, Gao S, Yan H. Performance optimum analysis of an irreversible molten carbonate fuel cell–Stirling heat engine hybrid system. Energy 2014;64:923–30.
[22] Zhang X, Wang Y, Guo J, Shih T-M, Chen J. A unified model of high-temperature fuel-cell heat-engine hybrid systems and analyses of its optimum performances. Int J Hydrogen Energy 2014;39:1811–25.
[23] Zhao M, Zhang H, Hu Z, Zhang Z, Zhang J. Performance characteristics of a direct carbon fuel cell/thermoelectric generator hybrid system. Energy Convers Manage 2015;89:683–9.
[24] Yang P, Zhang H. Parametric analysis of an irreversible proton exchange membrane fuel cell/absorption refrigerator hybrid system. Energy 2015;85:458–67.
[25] Chen X, Wang Y, Cai L, Zhou Y. Maximum power output and load matching of a phosphoric acid fuel cell-thermoelectric generator hybrid system. J Power Sources 2015;294:430–6.
[26] Zhang X, Liu H, Ni M, Chen J. Performance evaluation and parametric optimum design of a syngas molten carbonate fuel cell and gas turbine hybrid system. Renew Energy 2015;80:407–14.
[27] Yang P, Zhang H, Hu Z. Parametric study of a hybrid system integrating a phosphoric acid fuel cell with an absorption refrigerator for cooling purposes. Int J Hydrogen Energy 2016;41:3579–90.
[28] Huang C, Pan Y, Wang Y, Su G, Chen J. An efficient hybrid system using a thermionic generator to harvest waste heat from a reforming molten carbonate fuel cell. Energy Convers Manage 2016;121:186–93.
[29] Chen X, Wang Y, Zhao Y, Zhou Y. A study of double functions and load matching of a phosphoric acid fuel cell/heat-driven refrigerator hybrid system. Energy 2016;101:359–65.
[30] Açıkkalp E. Performance analysis of irreversible molten carbonate fuel cell–Braysson heat engine with ecological objective approach. Energy Convers Manage 2017;132:432–7.
[31] Sánchez D, Chacartegui R, Jiménez-Espadafor F, Sánchez T. A new concept for high temperature fuel cell hybrid systems using supercritical carbon dioxide. J Fuel Cell Sci Technol 2009;6:021306.
[32] Sanchez D, de Escalona JM, Chacartegui R, Munoz A, Sanchez T. A comparison between molten carbonate fuel cells based hybrid systems using air and supercritical carbon dioxide Brayton cycles with state of the art technology. J Power Sources 2011;196:4347–54.
[33] Baronci A, Messina G, McPhail SJ, Moreno A. Numerical investigation of a MCFC (Molten Carbonate Fuel Cell) system hybridized with a supercritical CO_2 Brayton cycle and compared with a bottoming Organic Rankine Cycle. Energy 2015;93:1063–73.
[34] Mahmoudi S, Ghavimi A. Thermoeconomic analysis and multi objective optimization of a molten carbonate fuel cell–supercritical carbon dioxide–organic Rankin cycle integrated power system using liquefied natural gas as heat sink. Appl Therm Eng 2016;107:1219–32.
[35] Mehrpooya M, Bahramian P, Pourfayaz F, Rosen MA. Introducing and analysis of a hybrid molten carbonate fuel cell-supercritical carbon dioxide Brayton cycle system. Sustain Energy Technol Assess 2016;18:100–6.
[36] Ahmadi MH, Ahmadi MA, Sadatsakkak SA. Thermodynamic analysis and performance optimization of irreversible Carnot refrigerator by using multi-objective evolutionary algorithms (MOEAs). Renew Sustain Energy Rev 2015;51:1055–70.
[37] Açıkkalp E. Exergetic sustainability evaluation of irreversible Carnot refrigerator. Physica A 2015;436:311–20.
[38] Chen L, Sun F, Wu C, Kiang R. Theoretical analysis of the performance of a regenerative closed Brayton cycle with internal irreversibilities. Energy Convers Manage 1997;38:871–7.
[39] Chen L, Wang W, Sun F, Wu C. Closed intercooled regenerator Brayton-cycle with constant-temperature heat-reservoirs. Appl Energy 2004;77:429–46.
[40] Chen L, Feng H, Sun F. Exergoeconomic performance optimization for a combined cooling, heating and power generation plant with an endoreversible closed Brayton cycle. Math Comput Model 2011;54:2785–801.
[41] Zhang Z, Chen L, Yang B, Ge Y, Sun F. Thermodynamic analysis and optimization of an air Brayton cycle for recovering waste heat of blast furnace slag. Appl Therm Eng 2015;90:742–8.
[42] Ahmadi MH, Ahmadi M-A, Pourfayaz F, Bidi M. Thermodynamic analysis and optimization for an irreversible heat pump working on reversed Brayton cycle. Energy Convers Manage 2016;110:260–7.
[43] Yang B, Chen L, Sun F. Exergetic performance optimization of an endoreversible variable-temperature heat reservoirs intercooled regenerated Brayton cogeneration plant. J Energy Inst 2016;89:1–11.
[44] Ahmadi MH, Ahmadi M-A, Pourfayaz F. Performance assessment and optimization of an irreversible nano-scale Stirling engine cycle operating with Maxwell-Boltzmann gas. Eur Phys J Plus 2015;130:1–13.
[45] Feng H, Chen L, Xie Z, Sun F. Constructal optimization for a single tubular solid oxide fuel cell. J Power Sources 2015;286:406–13.

[46] Chen L, Wu C, Sun F. Finite time thermodynamic optimization or entropy generation minimization of energy systems. J Non-Equilib Thermodyn 1999;24:327–59.
[47] Wu C. Recent advances in finite-time thermodynamics. Nova Publishers; 1999.
[48] Chen L. Advances in finite time thermodynamics: analysis and optimization. Nova Publishers; 2004.
[49] Açıkkalp E. Methods used for evaluation of actual power generating thermal cycles and comparing them. Int J Electr Power Energy Syst 2015;69:85–9.
[50] Ahmadi MH, Ahmadi MA, Pourfayaz F. Thermodynamic analysis and evolutionary algorithm based on multi-objective optimization performance of actual power generating thermal cycles. Appl Therm Eng 2016;99:996–1005.
[51] Ahmadi MH, Mehrpooya M, Pourfayaz F. Exergoeconomic analysis and multi objective optimization of performance of a Carbon dioxide power cycle driven by geothermal energy with liquefied natural gas as its heat sink. Energy Convers Manage 2016;119:422–34.
[52] Chen L, Xia S. Generalized thermodynamic dynamic-optimization for irreversible cycles. Beijing: Science Press; 2016.
[53] Chen L, Feng H, Xie Z. Generalized thermodynamic optimization for iron and steel production processes: theoretical exploration and application cases. Entropy 2016;18:353.
[54] Özel G, Açıkkalp E, Savaş AF, Yamık H. Comparative analysis of thermoeconomic evaluation criteria for an actual heat engine. J Non-Equilib Thermodyn 2016;41:225–35.
[55] Chen L, Xia S. Generalized thermodynamic dynamic-optimization for irreversible processes. Beijing: Science Press; 2016.
[56] Angulo-Brown F. An ecological optimization criterion for finite-time heat engines. J Appl Phys 1991;69:7465–9.
[57] Yan Z. Comment on "ecological optimization criterion for finite-time heat engines". J Appl Phys 1993;73:3583.
[58] Cheng C-Y. Ecological optimization of an endoreversible Brayton cycle. Energy Convers Manage 1998;39:33–44.
[59] Cheng C-Y. Ecological optimization of an irreversible Brayton heat engine. J Phys D Appl Phys 1999;32:350.
[60] Tu Y, Chen L, Sun F, Wu C. Exergy-based ecological optimisation for an endoreversible Brayton refrigeration cycle. Int J Exergy 2006;3:191–201.
[61] Chen L, Zhu X, Sun F, Wu C. Exergy-based ecological optimization of linear phenomenological heat-transfer law irreversible Carnot-engines. Appl Energy 2006;83:573–82.
[62] Zhang W, Chen L, Sun F, Wu C. Exergy-based ecological optimal performance for a universal endoreversible thermodynamic cycle. Int J Ambient Energy 2007;28:51–6.
[63] Chen L, Zhang W, Sun F. Power, efficiency, entropy-generation rate and ecological optimization for a class of generalized irreversible universal heat-engine cycles. Appl Energy 2007;84:512–25.
[64] Ding Z, Chen L, Sun F. Ecological optimization of energy selective electron (ESE) heat engine. Appl Math Model 2011;35:276–84.
[65] Chen L, Liu X, Ge Y, Wu F, Sun F. Ecological optimisation of irreversible harmonic oscillator Carnot refrigerator. J Energy Inst 2013;86:85–96.
[66] Chen L, Wu X, Xiao Q, Ge Y, Sun F. Local stability of a generalized irreversible Carnot engine working at the maximum ecological function. Environ Eng Manage J (EEMJ) 2015;14.
[67] Li Y, Liu G, Liu X, Liao S. Thermodynamic multi-objective optimization of a solar-dish Brayton system based on maximum power output, thermal efficiency and ecological performance. Renew Energy 2016;95:465–73.
[68] Zhou J, Chen L, Ding Z, Sun F. Analysis and optimization with ecological objective function of irreversible single resonance energy selective electron heat engines. Energy 2016;111:306–12.
[69] Midilli A, Dincer I. Development of some exergetic parameters for PEM fuel cells for measuring environmental impact and sustainability. Int J Hydrogen Energy 2009;34:3858–72.
[70] Midilli A, Kucuk H, Dincer I. Environmental and sustainability aspects of a re-circulating aquaculture system. Environ Prog Sustain Energy 2012;31:604–11.
[71] Bozoglan E, Midilli A, Hepbasli A. Sustainable assessment of solar hydrogen production techniques. Energy 2012;46:85–93.
[72] Aydin H. Exergetic sustainability analysis of LM6000 gas turbine power plant with steam cycle. Energy 2013;57:766–74.
[73] Aydın H, Turan Ö, Karakoç TH, Midilli A. Exergo-sustainability indicators of a turboprop aircraft for the phases of a flight. Energy 2013;58:550–60.
[74] Aydın H, Turan O, Karakoc TH, Midilli A. Sustainability assessment of PW6000 turbofan engine: an exergetic approach. Int J Exergy 2014;14:388–412.
[75] Açıkkalp E, Caner N. Application of exergetic sustainability index to a nano-scale irreversible Brayton cycle operating with ideal Bose and Fermi gasses. Phys Lett A 2015;379:1990–7.
[76] Açıkkalp E, Caner N. Application of exergetic sustainable index to the quantum irreversible Diesel refrigerator cycles for 1D box system. Eur Phys J Plus 2015;130:73.
[77] Aydin H, Turan O, Karakoc TH, Midilli A. Exergetic sustainability indicators as a tool in commercial aircraft: a case study for a turbofan engine. Int J Green Energy 2015;12:28–40.
[78] Dalkıran A, Açıkkalp E, Caner N. Analysis of a quantum irreversible Otto cycle with exergetic sustainable index. Physica A 2016;453:316–26.
[79] Açıkkalp E, Savaş AF, Caner N, Yamık H. Assessment of nano-scale Stirling refrigerator using working fluid as Maxwell-Boltzmann gases by thermo-ecological and sustainability criteria. Chem Phys Lett 2016;658:303–8.
[80] Ekici S, Sohret Y, Coban K, Altuntas O, Karakoc TH. Sustainability metrics of a small scale turbojet engine. Int J Turbo & Jet-Engines 2016.
[81] Ombuki B, Ross BJ, Hanshar F. Multi-objective genetic algorithms for vehicle routing problem with time windows. Appl Int 2006;24:17–30.
[82] Blecic I, Cecchini A, Trunfio GA. A decision support tool coupling a causal model and a multi-objective genetic algorithm. Appl Int 2007;26:125–37.
[83] Özyer T, Zhang M, Alhajj R. Integrating multi-objective genetic algorithm based clustering and data partitioning for skyline computation. Appl Int 2011;35:110–22.
[84] Zuo H, Luo Z, Guan J, Wang Y. Multidisciplinary design optimization on production scale of underground metal mine. J Central South Univ 2013;20:1332–40.
[85] Zhang B, E J, Gong J, Yuan W, Zuo W, Li Y, et al. Multidisciplinary design optimization of the diesel particulate filter in the composite regeneration process. Appl Energy 2016;181:14–28.
[86] Van Veldhuizen DA, Lamont GB. Multiobjective evolutionary algorithms: analyzing the state-of-the-art. Evol Comput 2000;8:125–47.
[87] Konak A, Coit DW, Smith AE. Multi-objective optimization using genetic algorithms: a tutorial. Reliab Eng Syst Saf 2006;91:992–1007.
[88] Lotfan S, Ghiasi RA, Fallah M, Sadeghi M. ANN-based modeling and reducing dual-fuel engine's challenging emissions by multi-objective evolutionary algorithm NSGA-II. Appl Energy 2016;175:91–9.
[89] Toffolo A, Lazzaretto A. Evolutionary algorithms for multi-objective energetic and economic optimization in thermal system design. Energy 2002;27:549–67.
[90] Lazzaretto A, Toffolo A. Energy, economy and environment as objectives in multi-criterion optimization of thermal systems design. Energy 2004;29:1139–57.
[91] Autissier N, Palazzi F, Maréchal F, Van Herle J, Favrat D. Thermo-economic optimization of a solid oxide fuel cell, gas turbine hybrid system. J Fuel Cell Sci Technol 2007;4:123–9.
[92] Ahmadi MH, Hosseinzade H, Sayyaadi H, Mohammadi AH, Kimiaghalam F. Application of the multi-objective optimization method for designing a powered Stirling heat engine: design with maximized power, thermal efficiency and minimized pressure loss. Renew Energy 2013;60:313–22.
[93] Ahmadi MH, Sayyaadi H, Mohammadi AH, Barranco-Jimenez MA. Thermo-economic multi-objective optimization of solar dish-Stirling engine by implementing evolutionary algorithm. Energy Convers Manage 2013;73:370–80.
[94] Ahmadi MH, Sayyaadi H, Dehghani S, Hosseinzade H. Designing a solar powered Stirling heat engine based on multiple criteria: maximized thermal efficiency and power. Energy Convers Manage 2013;75:282–91.
[95] Ahmadi MH, Dehghani S, Mohammadi AH, Feidt M, Barranco-Jimenez MA. Optimal design of a solar driven heat engine based on thermal and thermo-economic criteria. Energy Convers Manage 2013;75:635–42.
[96] Ahmadi MH, Mohammadi AH, Dehghani S. Evaluation of the maximized power of a regenerative endoreversible Stirling cycle using the thermodynamic analysis. Energy Convers Manage 2013;76:561–70.
[97] Ahmadi MH, Mohammadi AH, Dehghani S, Barranco-Jimenez MA. Multi-objective thermodynamic-based optimization of output power of Solar Dish-Stirling engine by implementing an evolutionary algorithm. Energy Convers Manage 2013;75:438–45.
[98] Toghyani S, Kasaeian A, Ahmadi MH. Multi-objective optimization of Stirling engine using non-ideal adiabatic method. Energy Convers Manage 2014;80:54–62.
[99] Ahmadi MH, Ahmadi MA, Mohammadi AH, Feidt M, Pourkiaei SM. Multi-objective optimization of an irreversible Stirling cryogenic refrigerator cycle. Energy Convers Manage 2014;82:351–60.
[100] Ahmadi MH, Ahmadi M-A, Mohammadi AH, Mehrpooya M, Feidt M. Thermodynamic optimization of Stirling heat pump based on multiple criteria. Energy Convers Manage 2014;80:319–28.
[101] Sayyaadi H, Ahmadi MH, Dehghani S. Optimal design of a solar-driven heat engine based on thermal and ecological criteria. J Energy Eng 2014;141:04014012.
[102] Ahmadi MH, Ahmadi M-A, Mehrpooya M, Hosseinzade H, Feidt M. Thermodynamic and thermo-economic analysis and optimization of performance of irreversible four-temperature-level absorption refrigeration. Energy Convers Manage 2014;88:1051–9.
[103] Ahmadi MH, Ahmadi MA. Thermodynamic analysis and optimization of an irreversible Ericsson cryogenic refrigerator cycle. Energy Convers Manage 2015;89:147–55.
[104] Ahmadi MH, Ahmadi MA, Mehrpooya M, Sameti M. Thermo-ecological analysis and optimization performance of an irreversible three-heat-source absorption heat pump. Energy Convers Manage 2015;90:175–83.
[105] Ahmadi MH, Ahmadi MA, Bayat R, Ashouri M, Feidt M. Thermo-economic optimization of Stirling heat pump by using non-dominated sorting genetic algorithm. Energy Convers Manage 2015;91:315–22.
[106] Sahraie H, Mirani MR, Ahmadi MH, Ashouri M. Thermo-economic and thermodynamic analysis and optimization of a two-stage irreversible heat pump. Energy Convers Manage 2015;99:81–91.
[107] Ahmadi MH, Ahmadi M-A, Feidt M. Thermodynamic analysis and evolutionary algorithm based on multi-objective optimization of performance for irreversible four-temperature-level refrigeration. Mech Ind 2015;16:207.
[108] Sadatsakkak SA, Ahmadi MH, Ahmadi MA. Thermodynamic and thermo-economic analysis and optimization of an irreversible regenerative closed Brayton cycle. Energy Convers Manage 2015;94:124–9.
[109] Mamaghani AH, Najafi B, Shirazi A, Rinaldi F. Exergetic, economic, and environmental evaluations and multi-objective optimization of a combined molten carbonate fuel cell-gas turbine system. Appl Therm Eng 2015;77:1–11.
[110] Ahmadi MH, Mehrpooya M. Thermo-economic modeling and optimization of an irreversible solar-driven heat engine. Energy Convers Manage 2015;103:616–22.
[111] Sadatsakkak SA, Ahmadi MH, Bayat R, Pourkiaei SM, Feidt M. Optimization density power and thermal efficiency of an endoreversible Braysson cycle by using non-dominated sorting genetic algorithm. Energy Convers Manage 2015;93:31–9.

[112] Ahmadi MH, Ahmadi MA, Shafaei A, Ashouri M, Toghyani S. Thermodynamic analysis and optimization of the Atkinson engine by using NSGA-II. Int J Low-Carbon Technol 2016;11:317–24.
[113] Ahmadi MH, Ahmadi MA, Mellit A, Pourfayaz F, Feidt M. Thermodynamic analysis and multi objective optimization of performance of solar dish Stirling engine by the centrality of entransy and entropy generation. Int J Electr Power Energy Syst 2016;78:88–95.
[114] Ahmadi MH, Ahmadi MA, Feidt M. Performance optimization of a solar-driven multi-step irreversible brayton cycle based on a multi-objective genetic algorithm. Oil Gas Sci Technol-Revue d'IFP Energies nouvelles 2016;71:16.
[115] Ahmadi MH, Ahmadi MA. Multi objective optimization of performance of three-heat-source irreversible refrigerators based algorithm NSGAII. Renew Sustain Energy Rev 2016;60:784–94.
[116] Ahmadi MH, Mohammadi AH, Pourkiaei SM. Optimisation of the thermodynamic performance of the Stirling engine. Int J Ambient Energy 2016;37:149–61.
[117] Ahmadi MH, Ahmadi M-A, Mehrpooya M, Feidt M, Rosen MA. Optimal design of an Otto cycle based on thermal criteria. Mech Ind 2016;17:111.
[118] Ganjehkaviri A, Jaafar MM, Hosseini S, Barzegaravval H. On the optimization of energy systems: results utilization in the design process. Appl Energy 2016;178:587–99.
[119] Ahmadi MH, Nabakhteh MA, Ahmadi M-A, Pourfayaz F, Bidi M. Investigation and optimization of performance of nano-scale Stirling refrigerator using working fluid as Maxwell-Boltzmann gases. Physica A 2017;483:337–50.
[120] Ahmadi MH, Ahmadi M-A, Maleki A, Pourfayaz F, Bidi M, Açıkkalp E. Exergetic sustainability evaluation and multi-objective optimization of performance of an irreversible nanoscale Stirling refrigeration cycle operating with Maxwell-Boltzmann gas. Renew Sustain Energy Rev 2017;78:80–92.
[121] Sameti M, Haghighat F. Optimization approaches in district heating and cooling thermal network. Energy Build 2017;140:121–30.
[122] Biswas PP, Suganthan P, Amaratunga GA. Decomposition based multi-objective evolutionary algorithm for windfarm layout optimization. Renew Energy 2017.
[123] Açıkkalp E. Ecologic and sustainable objective thermodynamic evaluation of molten carbonate fuel cell–supercritical CO_2 Brayton cycle hybrid system. Int J Hydrogen Energy 2017;42:6272–80.
[124] Holland JH. Adaptation in natural and artificial systems: an introductory analysis with applications to biology, control, and artificial intelligence. MIT Press; 1992.
[125] Pirkandi J, Jokar MA, Sameti M, Kasaeian A, Kasaeian F. Simulation and multi-objective optimization of a combined heat and power (CHP) system integrated with low-energy buildings. J Build Eng 2016;5:13–23.
[126] Sameti M, Jokar MA, Astaraei FR. Prediction of solar Stirling power generation in smart grid by GA-ANN model. Int J Comput Appl Technol 2017;55:147–57.
[127] MATLAB, MathWorks. Available: < https://www.mathworks.com/products/matlab.html > .